Combined dark matter search towards dwarf spheroidal galaxies with *Fermi*-LAT, HAWC, H.E.S.S., MAGIC, and VERITAS

Journal of Cosmology and Astroparticle Physics
An IOP and SISSA journal

Received: *December 20, 2024*
Revised: *August 4, 2025*
Accepted: *August 16, 2025*
Published: *March 11, 2026*

Combined dark matter search towards dwarf spheroidal galaxies with *Fermi*-LAT, HAWC, H.E.S.S., MAGIC, and VERITAS

The Fermi-LAT collaboration, the HAWC collaboration, the H.E.S.S. collaboration, the MAGIC collaboration and the VERITAS collaboration

Full author list at the end of the paper

E-mail: contact.hess@hess-experiment.eu, contact.magic@mpp.mpg.de, echarles@slac.stanford.edu, dimauro.mattia@gmail.com, jpharding@lanl.gov, salaza82@msu.edu, tollefs2@msu.edu, chiara.giuri@desy.de, elisa.pueschel@astro.rub.de

Abstract: Dwarf spheroidal galaxies (dSphs) are excellent targets for indirect dark matter (DM) searches using gamma-ray telescopes because they are thought to have high DM content and a low astrophysical background. The sensitivity of these searches is improved by combining the observations of dSphs made by different gamma-ray telescopes. We present the results of a combined search by the most sensitive currently operating gamma-ray telescopes, namely: the satellite-borne *Fermi*-LAT telescope; the ground-based imaging atmospheric Cherenkov telescope arrays H.E.S.S., MAGIC, and VERITAS; and the HAWC water Cherenkov detector. Individual datasets were analyzed using a common statistical approach. Results were subsequently combined via a global joint likelihood analysis. We obtain constraints on the velocity-weighted cross section $\langle \sigma v \rangle$ for DM self-annihilation as a function of the DM particle mass. This five-instrument combination allows the derivation of up to 2-3 times more constraining upper limits on $\langle \sigma v \rangle$ than the individual results over a wide mass range spanning from 5 GeV to 100 TeV. Depending on the DM content modeling, the 95% confidence level observed limits reach 1.5×10^{-24} cm^{3}s^{-1} and 3.2×10^{-25} cm^{3}s^{-1}, respectively, in the $\tau^+\tau^-$ annihilation channel for a DM mass of 2 TeV.

Keywords: dark matter experiments, dwarfs galaxies, gamma ray experiments

https://doi.org/10.1088/1475-7516/2026/03/035

JCAP03(2026)035

Contents

1 Introduction

The observation of gamma rays from dark matter (DM) interactions would answer key questions about the nature of the Universe. Such a discovery would also shed light on our understanding of physics beyond the Standard Model (SM). According to the latest measurements of the energy content of the Universe, baryonic matter is observed to make up about 5% of the total energy content, with the rest being Cold Dark Matter (CDM) (27%) and dark energy (68%) [1]. Experimental evidence for DM can be found in observations of gravitational lensing [2], the large-scale structure of galaxies [3], the power spectrum of the cosmic microwave background [4], and the rotational velocity of galaxies [5], among other probes [6]. Assuming DM to be made of elementary particles, in most models they are considered to be electrically neutral, stable on cosmological time scales, and cold (i.e., non-relativistic). A well-motivated class of CDM candidate particles are the Weakly Interacting Massive Particles (WIMPs): elementary particles not contained in the SM, which may have been produced in the early Universe and that would annihilate or decay into SM particles. If we assume that a GeV–TeV mass scale particle, with weak-scale couplings, was decoupled from thermal equilibrium in the early Universe, such particles could reproduce the observed DM relic density [1, 7]. This coincidence between the predicted thermal abundance of WIMPs and the observed DM density is known as the "WIMP miracle" [8]. A precise computation

JCAP03(2026)035

of the thermally-averaged velocity-weighted annihilation cross section provides $\langle\sigma v\rangle_{\rm th} \simeq 2\times10^{-26}$ cm^{3}s^{-1} [9].

The primary WIMP DM search modes are: *direct detection* searches for signatures of the interaction of local DM particles in underground detectors; searches for DM particle *production* in accelerators such as the Large Hadron Collider at CERN; and the *indirect search* for DM decay or annihilation to SM products by ground-based and spaceborne observatories. In indirect searches, one looks for spatial and/or spectral signatures of DM annihilation or decay in the astrophysical fluxes of SM particles. Among those, gamma rays are detectable over a broad energy range with both spaceborne and ground-based astronomical observatories. They point back to their sources and are not subject to significant energy losses in the local universe. The aforementioned properties make gamma rays excellent probes for DM searches. Among the privileged targets for gamma-ray observations are the center of the Milky Way and its nearby satellite galaxies.

Dwarf spheroidal galaxies (dSphs) are groups of gravitationally bound stars with a typical radius of 10^2–10^3 pc. They host small amounts of visible mass (10^3–10^7 M$_\odot$) and show consequently low optical luminosities (10^3–10^7 L$_\odot$) [10]. The dSph satellites of the Milky Way are located at $\mathcal{O}$(100 kpc) Galactocentric distance, and mainly at high Galactic latitudes, although some of them lie closer to the Galactic plane, such as the Sagittarius dSph. Their kinematics tend to be dominated by random stellar motion, and the amplitude of the star motion is driven by the gravitational potential of the galaxy [11, 12]. The gas or dust content of dSphs is extremely low, and therefore cannot be used to trace the galactic dynamics [13]. The low luminosity of dSphs and their high mass-to-light ratio, compared to Milky-Way like galaxies, indicate that they are DM-dominated galaxies with negligible astrophysical background from gamma-ray emitters [14, 15]. The dSphs are therefore among the most promising targets for indirect DM searches using gamma-ray signals.

In this paper, we combine observations of dSphs performed with five different gamma-ray instruments, including satellite, water Cherenkov detector, and imaging atmospheric Cherenkov telescopes (IACTs) — *Fermi*-LAT, HAWC, H.E.S.S., MAGIC, and VERITAS — to search for DM signals. Our goal is to increase the sensitivity of indirect DM searches with gamma rays by using all available data on the selected objects over the widest possible DM mass range. Each of the instruments involved in the combination has accumulated large datasets of dSph observations. Each corresponding collaboration carried out analyses of the individual datasets. Then, a combined likelihood analysis with all their respective data was performed. This new combined study aims to extract more information from already independently analyzed data and to increase our chance of a possible DM detection. For this work, each collaboration analysis of their own datasets was done using common DM spectral and morphological models and common conventions on the statistical analysis, including the treatment of the relevant statistical uncertainties. This standardization avoids the need to share low-level experimental data (event lists) and instrument response functions (IRFs). Each collaboration computed a likelihood function versus the velocity-weighted cross section $\langle\sigma v\rangle$, scanning over the DM particle masses for several annihilation channels and each observed target. The obtained likelihood values were subsequently shared and combined into a global joint likelihood function, from which constraints on $\langle\sigma v\rangle$ were derived. This methodology was

JCAP03(2026)035

applied before in the previous combined DM search towards dSph galaxies by MAGIC and *Fermi*-LAT [16]. Those data constitute a subset of the dataset included in the present work.

This article is organized as follows: in section 2, we present the five collaborations that have participated in the combination and their observational datasets. In section 3 we recall the signal expected from DM annihilation, its dependence on the DM distribution in dSphs, and the associated uncertainties. In section 4 we describe the likelihood analysis technique and the procedure to combine the results. We present the results in section 5 and discuss and conclude in section 6.

2 Observations and data

In this section, we provide details about the sources observed, the detectors, and their associated datasets, which are also summarized in table 1. In general, we restricted the dSph observations included from *Fermi*-LAT and HAWC based on the intersection of dSphs studied in the two independent sets of J-factor calculations used in this work (see section 3 for more details). Even more stringent exclusion limits, especially at the lowest DM masses, could be obtained by including all known dSphs. However, since through our selection the known dSphs with the largest expected DM-induced gamma-ray flux are already included, we expect this improvement to be minor with respect to the results presented in section 5.

2.1 *Fermi*-LAT

The Large Area Telescope onboard the NASA *Fermi* satellite (*Fermi*-LAT) is a pair conversion telescope orbiting the Earth at an altitude of ~ 550 km [17]. It is sensitive to gamma rays in the energy range from 20 MeV to > 1 TeV. *Fermi*-LAT covers the lowest energy region of this study. *Fermi*-LAT has a wide field of view covering about 20% of the sky, and scans the whole sky approximately every 3 hours. The instrument detects gamma rays via pair conversion of the incoming photon to an electron and positron within the detector. Similar to particle accelerator experiments, the direction of these particles is recorded in a silicon strip tracker and the energy deposited in a cesium iodide calorimeter. Detailed descriptions of the detector and its performance can be found in [18]. The energy resolution of *Fermi*-LAT at 1 GeV is 10% and it reaches its minimum at 10 GeV, where it is 5%. The 68% containment radius angular resolution for one photon is 1° (0.2°) at 1 GeV (> 10 GeV). An overview of the dSphs observed by *Fermi*-LAT and a DM search using these observations is given in [19].

We analyze almost ten years of Pass 8 [20, 21] data (data processing `P8R2`) from August 2008 to March 2018. We select `SOURCE` class events, passing the basic quality filter cuts, and their corresponding `P8R2_SOURCEVETO_V2` IRFs [22]. We choose energies between 300 MeV and 1 TeV and apply a cut to zenith angles $< 100°$ between 300 MeV and 1 GeV and $< 105°$ above 1 GeV in order to exclude contamination from the Earth's limb. We model the background with sources reported in the *Fermi*-LAT 8-year source catalog (4FGL) [23]. We also include in the model the latest released interstellar emission model (IEM), namely `gll_iem_v07.fits`,[1] and its corresponding isotropic template `iso_P8R2_SOURCEVETO_V2_v1.txt`. We analyze

[1] A complete discussion about this new IEM can be found at https://fermi.gsfc.nasa.gov/ssc/data/analysis/software/aux/4fgl/Galactic_Diffuse_Emission_Model_for_the_4FGL_Catalog_Analysis.pdf.

JCAP03(2026)035

the $12^\circ \times 12^\circ$ regions of interest centered on the locations of the dSphs and choose a pixel size of 0.08°. We include in the background model sources located in a region $14^\circ \times 14^\circ$ in order to include also sources at most 1° outside our region of interest. We apply the same analysis performed on dSphs in [19, 24, 25] by employing versions `0.18.0` of `Fermipy` and `1.2.3` of the `Fermitools`.[2]

2.2 HAWC

The High-Altitude Water Cherenkov (HAWC) observatory is a high-energy gamma-ray detector located at Sierra Negra, Mexico. The site is 4100 m above sea level, at latitude and longitude (19.0° N, 97.3° W). HAWC is a survey instrument with a wide field of view, and observes two thirds of the sky every day within declinations of -20.0° to 60.0° [26]. It is sensitive to gamma-ray energies between 300 GeV and >100 TeV [27], with 30–100% energy resolution. HAWC is an array of 300 water Cherenkov detectors (WCD) covering a 22,000 m^2 area. When a cosmic particle enters the atmosphere and interacts, it initiates an air shower, the particles of which travel through the HAWC WCDs, emitting Cherenkov light in the water. The Cherenkov light is detected by the photo-multiplier tubes (PMTs) in the WCDs [27]. The timing and intensity of the Cherenkov light detected by the different PMTs across the HAWC array is used to determine the incident angle, energy, and species of the initiating cosmic particle [27]. The HAWC sensitivity in this analysis depends on the spectrum of the source, and its angular resolution (68% containment) varies from 1° at 1 TeV to 0.2° at >30 TeV [27].

For this analysis, HAWC reconstructs gamma-ray energies from the fraction of PMTs hit on the array [27]. HAWC has been operated as a partial detector since August 2013 and with the full detector since March 2015. HAWC provides data corresponding to 1038 days of livetime starting on November 26, 2014. The exposure to each dSph depends on the declination of the source with respect to the latitude of HAWC (see HAWC's exposure to all dSphs included in this analysis in table 1). The background is estimated through HAWC's direct integration method [27] with the region of interest around the dSphs set at 4°. HAWC used `HAL` and `threeML` public software for its analysis framework [28]. In this work, the dSphs are treated as extended sources in HAWC data and analyzed following the methods presented in [29].

2.3 H.E.S.S.

The High Energy Stereoscopic System (H.E.S.S.) is an array of five IACTs situated at an altitude of 1800 m (23.3° S, 16.5° E) in the Khomas Highland of Namibia, sensitive to gamma rays from $\sim$ 50 GeV to $\sim$ 100 TeV. Four 12-m diameter telescopes (CT1-4) are positioned at the corners of a 120-m side square, and one 28-m diameter telescope (CT5) is located at the center of the array. The observations used in this work are taken in wobble mode [30] where the telescope pointing alternates directions with an offset of 0.7° from the target position. Standard quality selection procedures are applied to the data [31]. After the calibration of the raw data, the events are reconstructed using a template-fitting technique in which the images recorded in the cameras are compared to shower templates computed from a semi-analytical model [32]. This technique achieves an energy resolution of 10% and an angular resolution

[2] https://fermi.gsfc.nasa.gov/ssc/data/analysis/.

JCAP03(2026)035

of 0.06°at 68% containment radius for gamma-ray energies above 200 GeV for the CT1-4 array, with a field of view of 5°. The point-source 5σ flux sensitivity is about 1% of the Crab Nebula flux for 25 h of observations near zenith [31].

H.E.S.S. data include observations of the dSphs Carina, Coma Berenices, Fornax, and Sculptor. Data were collected with the CT1-4 telescope array, requiring at least two telescopes to detect the same air shower. For each dSph, the signal region, referred to as the ON region, is defined as a disk centered at the nominal position of the dSph with a radius of 0.1°. We estimate the background contribution in the ON regions using several background-control (or OFF) regions of the same size, shape and angular distance from the pointing position as the corresponding ON region [33]. This method guarantees almost identical acceptances in the ON and OFF regions, such that no further offline background normalization is necessary. H.E.S.S. follows the recommended statistical approach of [34] to derive the excess significances provided in table 1.

Sculptor and Carina [35–37] were observed between January 2008 and December 2009. Coma Berenices and Fornax [36, 37] were observed from 2010 to 2013 and in 2010, respectively. The pointing offset in the case of Fornax is larger, since it was not the primary target of the corresponding dataset. The observation time of the four dSphs analyzed in this paper amounts to 54 h. The data are independently analyzed with the H.E.S.S. official software packages `ParisAnalysis` [32], and `HAP` [38] for analysis result crosschecks.

2.4 MAGIC

The *Florian Goebel* Major Atmospheric Gamma-ray Imaging Cherenkov (MAGIC) telescopes are located at the Roque de los Muchachos Observatory (28.8° N, 17.9° W, 2200 m above sea level) on the Canary Island of La Palma, Spain. MAGIC consists of two IACTs, each with a 17-m reflector diameter and equipped with fast imaging cameras with a 3.5° field of view. MAGIC is sensitive to gamma rays above $\gtrsim 30$ GeV. The 5σ sensitivity above 220 GeV for 50 h of observations of a point-like source is $\sim 0.7\%$ of the flux of the Crab Nebula, with an associated energy resolution of $\sim 16\%$ and a 0.07° angular resolution measured as the 68% containment radius of the gamma-ray excess [39].

MAGIC provides data from four dSphs observed with the full two-telescope MAGIC system: Segue 1 [40], Ursa Major II [41], Draco, and Coma Berenices [42]. In total, a 354 h dataset was collected in wobble mode [30] with two pointing positions, offset by 0.4° from the center of the target, used for each source. In the MAGIC analysis, the size of the ON and the respective OFF regions are optimized for each source to increase the sensitivity to a potential DM signal (see [41] for more details). Observations of Segue 1 were taken between 2011 and 2013 and represent the deepest IACT observation of any dSph to date. Ursa Major II, Draco, and Coma Berenices were observed between 2014 and 2016, March to September 2018, and January to June 2019, respectively. MAGIC hardware upgrades such as [43] and changes in the telescope reflectivity define distinct periods of data taking, each of which is analyzed using an individual set of IRFs obtained from dedicated Monte Carlo simulations. The data are reduced with the standard `MARS` analysis software [44].

JCAP03(2026)035

2.5 VERITAS

The Very Energetic Radiation Imaging Telescope Array System (VERITAS) instrument is an array of four ground-based IACTs with 12-m focal length placed $\sim$ 100 m from each other. VERITAS is situated at the Fred Lawrence Whipple Observatory in southern Arizona, (31.7°N, 111.0°W), 1300 m above sea level. VERITAS has been operational since 2007. The total field of view is $\sim 3.5°$. VERITAS is most sensitive in the very-high-energy band, from $\sim 85\,\mathrm{GeV}$ up to $\sim 30\,\mathrm{TeV}$. Its energy resolution is $\sim 15\%$, and its angular resolution in terms of the 68% containment radius is $< 0.1°$ per event at 1 TeV. Its sensitivity is such that a point-like source with 1% of the flux of the Crab Nebula can be detected within 25 h at zenith angles smaller than 30° [45].

For this analysis, VERITAS provides data for four dSphs in the Northern Hemisphere: Boötes I, Draco, Segue 1, and Ursa Minor. The targets were observed from 2009 to 2013 for ~ 216 h [46]. Data were collected in wobble pointing mode [30], with 0.5° between the camera center and the source position.

Loose event selection criteria are used in order to keep the energy threshold as low as possible, increasing the sensitivity to a potential DM signal at low energy. The analysis incorporated into this work adopted a $\theta < 0.17°$ cut on the angular distance of the reconstructed shower arrival position with respect to the target position to define the ON region. A novel background estimation method is used [47], in which OFF events are extracted from an annular region centered on the tracking position rather than the target position. Gradients across the camera are taken into account through a zenith-dependent acceptance function [48]. The `VEGAS` software pipeline for analysis and reconstruction [49] is used for this analysis.

3 Dark Matter signal

The differential flux of gamma rays of self-annihilating Majorana DM particles from an astrophysical source is [50]:

$$\frac{\mathrm{d}^2\Phi\left(\langle\sigma v\rangle, J\right)}{\mathrm{d}E\mathrm{d}\Omega} = \left(\frac{\langle\sigma v\rangle}{2m_{\mathrm{DM}}^2}\sum_f \mathrm{BR}_f \frac{\mathrm{d}N_f}{\mathrm{d}E}\right) \times \left(\frac{1}{4\pi}\frac{\mathrm{d}J}{\mathrm{d}\Omega}\right). \tag{3.1}$$

The first term of eq. 3.1 is the *particle physics factor* for DM annihilation, and depends on the thermally-averaged velocity-weighted cross section, $\langle\sigma v\rangle$, the mass of the DM particle, m_{DM}, and average differential spectrum of gamma rays per annihilation, $\mathrm{d}N_f/\mathrm{d}E$, for each final state f weighted by its branching ratio BR_f. We study seven annihilation channels with final states W^+W^-, ZZ, $b\bar{b}$, $t\bar{t}$, e^+e^-, $\mu^+\mu^-$, and $\tau^+\tau^-$ separately by assuming a 100% branching ratio in each case. The values considered for m_{DM} range from 5 GeV to 100 TeV, except for the W^+W^-, ZZ, and $t\bar{t}$ channels, where the range is from the corresponding kinematic threshold to 100 TeV. The $\mathrm{d}N_f/\mathrm{d}E$ spectrum is calculated according to [51] and includes electroweak corrections of the final state products (see appendix A).

The $\mathrm{d}J/\mathrm{d}\Omega$ term in eq. 3.1 is the *astrophysical factor*, or differential J-factor (see appendix B). The differential J-factor is proportional to the intensity of the expected DM annihilation gamma-ray signal from an astrophysical source as seen from Earth. The differential J-factor is defined as the integral of the square of the DM density distribution

JCAP03(2026)035

	Fermi-LAT	HAWC	H.E.S.S., MAGIC, VERITAS						
Source name	Exposure (10^{11} s cm^2)	$\lvert\Delta\phi\rvert$ (°)	IACTs	Zenith (°)	Time exposure (h)	Energy range (TeV)	$\theta_{\rm sig}$ (°)	τ	S (σ)
Boötes I	2.6	4.5	VERITAS	15 – 30	14.0	0.10–41	0.17	8.6	−1.0
Canes Venatici I	2.9	14.6	–	–	–	–	–	–	–
Canes Venatici II	2.9	15.3	–	–	–	–	–	–	–
Carina	3.1	–	H.E.S.S.	27 – 46	23.7	0.31–70	0.10	18.0	−0.3
Coma Berenices	2.7	4.9	H.E.S.S.	47 – 49	11.4	0.55–70	0.10	14.4	−0.4
			MAGIC	5–37	49.5	0.06–10	0.17	1.0	0.8
Draco	3.8	38.1	MAGIC	29–45	52.1	0.07–10	0.22	1.0	−0.7
			VERITAS	25 – 40	49.8	0.12–70	0.17	9.0	−1.0
Fornax	2.7	–	H.E.S.S.	11 – 25	6.8	0.23–70	0.10	45.5	−1.5
Hercules	2.8	6.3	–	–	–	–	–	–	–
Leo I	2.5	6.7	–	–	–	–	–	–	–
Leo II	2.6	3.1	–	–	–	–	–	–	–
Leo IV	2.4	19.5	–	–	–	–	–	–	–
Leo V	2.4	–	–	–	–	–	–	–	–
Leo T	2.6	–	–	–	–	–	–	–	–
Sculptor	2.7	–	H.E.S.S.	10 – 46	11.8	0.20–70	0.10	19.8	−2.2
Segue 1	2.5	2.9	MAGIC	13 – 37	158.0	0.06–10	0.12	1.0	−0.5
			VERITAS	15 – 35	92.0	0.08–50	0.17	7.6	0.7
Segue 2	2.7	–	–	–	–	–	–	–	–
Sextans	2.4	20.6	–	–	–	–	–	–	–
Ursa Major I	3.4	32.9	–	–	–	–	–	–	–
Ursa Major II	4.0	44.1	MAGIC	35 – 45	94.8	0.12–10	0.30	1.0	−2.1
Ursa Minor	4.1	–	VERITAS	35 – 45	60.4	0.16 – 93	0.17	8.4	−0.1

Table 1. Summary of dSph observations by each experiment used in this work. A '−' indicates the experiment did not observe this dSph or did not include its data on it for this study. For *Fermi*-LAT, the exposure at 1 GeV is given. For HAWC, $|\Delta\phi|$ is the absolute difference between the source declination and HAWC latitude, i.e. the zenith angle of the source at culmination. HAWC is more sensitive to sources with smaller $|\Delta\phi|$. For IACTs, we show the zenith angle range, the total exposure, the energy of the lowest and highest energy ON event considered for unbinned analysis and the lowest and highest energy bin edges considered for binned analysis, the angular radius $\theta_{\rm sig}$ of the signal or ON region, the ratio τ of exposures between the background-control (OFF) and signal (ON) regions, and the significance of gamma-ray excess, S(σ), in standard deviations.

$\rho_{\rm DM}$ along the line-of-sight (l.o.s.):

$$\frac{{\rm d}J}{{\rm d}\Omega} = \int_{\rm l.o.s.} \rho^2_{\rm DM}(r(s,\theta))\, ds, \tag{3.2}$$

where $\rho_{\rm DM}$ is assumed to be spherically symmetric and depends on the radial distance r from the center of the dSph. This distance can also be expressed in terms of the distance s from Earth along the l.o.s., and the angular distance, θ, with respect to the center of the dSph as $r^2(s,\theta) = s^2 + d^2 - 2sd\cos\theta$, where d is the distance between the Earth and the dSph nominal position. The total J-factor can then be obtained by integrating over the solid angle $\Delta\Omega$ corresponding to the dSph extension. We note that we use J-factors in the integrated form $J(\Delta\Omega)$ at a given angular radius θ for the remainder of this paper (see table 2), which reads:

$$J(\Delta\Omega) = \int_{\Delta\Omega}\int_{\rm l.o.s.} \rho^2_{\rm DM}(r(s,\theta))\, ds\, d\Omega. \tag{3.3}$$

The derivation of $\rho_{\rm DM}$ is performed through the Jeans analysis with the formalism of the spherical Jeans equation [12, 52–54]. This method allows the reconstruction of galactic dynamics based on spectroscopic data, assuming in the case of dSphs that the systems are in statistical equilibrium, non-rotating, and have a spherical symmetry.

In this study, we compute the limits on $\langle\sigma v\rangle$ from the combination of the dSph observations using two independent sets of J-factors produced by Geringer-Sameth et al. [53] (or $\mathcal{GS}$ set), and by Bonnivard et al. [52, 54] (or $\mathcal{B}$ set), respectively. We produce results from both $\mathcal{GS}$ and $\mathcal{B}$ sets to estimate the impact of the systematic uncertainty in the J-factor derivation. More details about the assumptions of each J-factor set can be found in appendix B, which also presents a comparison between the two sets of differential J-factors versus the angular radius of the integration region $\Delta\Omega$, measured from the dSph nominal position, for each of the twenty dSphs. A detailed review of the computation of J-factors can be found in [55]. The majority of J-factor estimations, especially for the DM-dominated dSphs, are compatible within uncertainties for the different sets of J-factors in the literature. Comparing the $\mathcal{GS}$ and $\mathcal{B}$ J-factors, the largest discrepancy occurs for the J-factor of Segue 1 (see table 2), because the analysis of the $\mathcal{B}$ set [54] is extremely sensitive to the inclusion or exclusion of a few marginal member stars [56]. Given that MAGIC and VERITAS have accumulated a wealth of observation time on Segue 1 and that the DM content of Segue 1 has been an active subject of debate [56], the usage of two different sets of J-factors in this work is well-motivated.[3]

Observations carried out by H.E.S.S. towards Sagittarius dSph [36, 59] amount to 90 hours. However, Sagittarius's relative proximity ($\sim$ 17 kpc) to the Galactic Center subjects it to tidal effects from the Milky Way. Determination of the DM distribution in this object is challenging [60], therefore H.E.S.S. observations of Sagittarius are not included in this study.

Ultra-faint Milky Way satellites have been recently unveiled by optical surveys in the southern hemisphere sky like PanSTARRS and DES. Of these, Reticulum II, Tucana II, Tucana III, Tucana IV and Grus II have been observed by H.E.S.S. [61]. The uncertainty on the DM distribution for ultra-faint systems is challenging to measure or predict. In

[3]We further note that the use of different J-factor calculations would result in different extracted limits on the velocity-weighted annihilation cross section. For instance, the J-factors derived in [57] weaken limits derived with *Fermi*-LAT data as well as those derived with VERITAS data [58].

JCAP03(2026)035

Name	Distance (kpc)	l, b (°)	$\log_{10} J$ ($\mathcal{GS}$ set) $\log_{10}(\mathrm{GeV^2 cm^{-5}})$	$\log_{10} J$ ($\mathcal{B}$ set) $\log_{10}(\mathrm{GeV^2 cm^{-5}})$
Boötes I	66	358.08, 69.62	$18.24^{+0.40}_{-0.37}$	$18.85^{+1.10}_{-0.61}$
Canes Venatici I	218	74.31, 79.82	$17.44^{+0.37}_{-0.28}$	$17.63^{+0.50}_{-0.20}$
Canes Venatici II	160	113.58, 82.70	$17.65^{+0.45}_{-0.43}$	$18.67^{+1.54}_{-0.97}$
Carina	105	260.11, −22.22	$17.92^{+0.19}_{-0.11}$	$18.02^{+0.36}_{-0.15}$
Coma Berenices	44	241.89, 83.61	$19.02^{+0.37}_{-0.41}$	$20.13^{+1.56}_{-1.08}$
Draco	76	86.37, 34.72	$19.05^{+0.22}_{-0.21}$	$19.42^{+0.92}_{-0.47}$
Fornax	147	237.10, −65.65	$17.84^{+0.11}_{-0.06}$	$17.85^{+0.11}_{-0.08}$
Hercules	132	28.73, 36.87	$16.86^{+0.74}_{-0.68}$	$17.70^{+1.08}_{-0.73}$
Leo I	254	225.99, 49.11	$17.84^{+0.20}_{-0.16}$	$17.93^{+0.65}_{-0.25}$
Leo II	233	220.17, 67.23	$17.97^{+0.20}_{-0.18}$	$18.11^{+0.71}_{-0.25}$
Leo IV	154	265.44, 56.51	$16.32^{+1.06}_{-1.70}$	$16.36^{+1.44}_{-1.65}$
Leo V	178	261.86, 58.54	$16.37^{+0.94}_{-0.87}$	$16.30^{+1.33}_{-1.16}$
Leo T	417	214.85, 43.66	$17.11^{+0.44}_{-0.39}$	$17.67^{+1.01}_{-0.56}$
Sculptor	86	287.53, −83.16	$18.57^{+0.07}_{-0.05}$	$18.63^{+0.14}_{-0.08}$
Segue 1	23	220.48, 50.43	$19.36^{+0.32}_{-0.35}$	$17.52^{+2.54}_{-2.65}$
Segue 2	35	149.43, −38.14	$16.21^{+1.06}_{-0.98}$	$19.50^{+1.82}_{-1.48}$
Sextans	86	243.50, 42.27	$17.92^{+0.35}_{-0.29}$	$18.04^{+0.50}_{-0.28}$
Ursa Major I	97	159.43, 54.41	$17.87^{+0.56}_{-0.33}$	$18.84^{+0.97}_{-0.43}$
Ursa Major II	32	152.46, 37.44	$19.42^{+0.44}_{-0.42}$	$20.60^{+1.46}_{-0.95}$
Ursa Minor	76	104.97, 44.80	$18.95^{+0.26}_{-0.18}$	$19.08^{+0.21}_{-0.13}$

Table 2. Summary of the relevant properties of the dSphs considered in the present work. Column 1 lists the dSphs. Columns 2 and 3 present their heliocentric distance and Galactic coordinates, respectively. Columns 4 and 5 report the J-factors of each object given by the independent $\mathcal{GS}$ and $\mathcal{B}$ studies and their estimated $\pm 1\sigma$ uncertainties. The values $\log_{10} J$ ($\mathcal{GS}$ set) correspond to the mean J-factor values for a dSph extension truncated at the outermost observed star. The values $\log_{10} J$ ($\mathcal{B}$ set) are provided for an extension ending at the tidal radius of each dSph.

addition to the uncertainty on the J-factor coming from the limited number of stellar tracers, the assumptions made to derive the J-factor value, such as a single stellar population, spherical symmetry, constant velocity anisotropy, or absence of tidal stripping, are expected to significantly impact the J-factor estimate for these systems. The selection of member stars for these ultra-faint systems is also complex due to the difficulty in distinguishing member stars from foreground stars. Therefore, the DES dSphs observed by H.E.S.S. are not considered in this study. Similarly, the ultra-faint satellite Triangulum II has been observed by HAWC [29] and MAGIC [62] but its seemingly high J-factor [63] may be overestimated due to the contamination of velocity dispersion measurements by binary systems. Further observations showed that the system may not be in equilibrium and may suffer from tidal disruption [64], which makes the determination of the DM distribution complex. Observations of Triangulum II are thus not considered in this study.

JCAP03(2026)035

4 Joint likelihood analysis

We conduct our DM search by means of a maximum likelihood analysis, in which we take advantage of the different spectral and morphological features expected for signal (see section 3) and background. Note that morphological features are treated differently in the analysis of each instrument and will be described later in this section.

We perform the derivation of our upper limits on $\langle\sigma v\rangle$ using the test statistic, TS, for each considered annihilation channel and DM mass:

$$\mathrm{TS} = -2\ln\lambda(\langle\sigma v\rangle), \tag{4.1}$$

where $\lambda(\langle\sigma v\rangle)$ is the profile likelihood ratio defined as a function of the annihilation cross section $\langle\sigma v\rangle$, which reads [65]:

$$\lambda\left(\langle\sigma v\rangle \mid \boldsymbol{\mathcal{D}}_{\mathrm{dSphs}}\right) = \frac{\mathcal{L}\left(\langle\sigma v\rangle; \hat{\hat{\boldsymbol{\nu}}} \mid \boldsymbol{\mathcal{D}}_{\mathrm{dSphs}}\right)}{\mathcal{L}\left(\widehat{\langle\sigma v\rangle}; \hat{\boldsymbol{\nu}} \mid \boldsymbol{\mathcal{D}}_{\mathrm{dSphs}}\right)}, \tag{4.2}$$

where $\boldsymbol{\mathcal{D}}_{\mathrm{dSphs}}$ is our set of observations, $\boldsymbol{\nu}$ represents the nuisance parameters, $\widehat{\langle\sigma v\rangle}$ and $\hat{\boldsymbol{\nu}}$ are the values that maximize $\mathcal{L}$ globally, and $\hat{\hat{\boldsymbol{\nu}}}$ is the set of values that maximize $\mathcal{L}$ for a given value of $\langle\sigma v\rangle$.

The *total* joint likelihood function $\mathcal{L}$ that describes all observations from all instruments and dSphs is factored into *partial* joint likelihood functions corresponding to each dSph l ($\mathcal{L}_{\mathrm{dSph},l}$) and its corresponding J-factor ($\mathcal{J}_l$):

$$\mathcal{L}\left(\langle\sigma v\rangle; \boldsymbol{\nu} \mid \boldsymbol{\mathcal{D}}_{\mathrm{dSphs}}\right) = \prod_{l=1}^{N_{\mathrm{dSphs}}} \mathcal{L}_{\mathrm{dSph},l}\left(\langle\sigma v\rangle; J_l, \boldsymbol{\nu_l} \mid \boldsymbol{\mathcal{D}_l}\right) \times \mathcal{J}_l\left(J_l \mid J_{l,\mathrm{obs}}, \sigma_{\log J_l}\right). \tag{4.3}$$

The quantity $N_{\mathrm{dSphs}} = 20$ is the number of dSphs considered in this work. $\boldsymbol{\mathcal{D}_l}$ is the set of gamma-ray observations for the l-th dSph; $\boldsymbol{\nu_l}$ is the set of nuisance parameters affecting the gamma-ray observations of the l-th dSph, excluding J_l. J_l is the total J-factor of the l-th dSph as defined in eq. 3.3; we treat it as an additional nuisance parameter. The quantities $\log_{10} J_{l,\mathrm{obs}}$ and $\sigma_{\log J_l}$ are obtained from fitting a log-normal function of $J_{l,\mathrm{obs}}$ to the posterior distribution of J_l [19]; their values are listed in table 2. Note that when $\sigma_{\log J_l}$ is asymmetric, the negative value was chosen as this results in a more conservative limit. The likelihood term $\mathcal{J}_l$ constraining the value of J_l can thus be written as:

$$\mathcal{J}_l\left(J_l \mid J_{l,\mathrm{obs}}, \sigma_{\log J_l}\right) = \frac{1}{\ln(10) J_{l,\mathrm{obs}}\sqrt{2\pi}\sigma_{\log J_l}} \exp\left(-\frac{\left(\log_{10} J_l - \log_{10} J_{l,\mathrm{obs}}\right)^2}{2\sigma^2_{\log J_l}}\right). \tag{4.4}$$

Both sets of J-factors in table 2 will be used independently in our analysis. Note that the right-hand side of eq. 4.4 is normalized such that it can be interpreted both as the likelihood function for J_l and as the probability density function (PDF) for the associated random variable $J_{l,\mathrm{obs}}$. Furthermore, the quantities $\langle\sigma v\rangle$ and J_l are degenerate in the computation of $\mathcal{L}_{\mathrm{dSph},l}$, which depends on $\frac{d\Phi}{dE}$ (see eq. 3.1). Therefore, as noted in [16], it is sufficient to compute $\mathcal{L}_{\mathrm{dSph},l}$ versus $\langle\sigma v\rangle$ for a fixed value of J_l. We use the $J_{l,\mathrm{obs}}(\mathcal{GS})$ reported in table 2 to perform the profiling of $\mathcal{L}$ with respect to J_l. The degeneracy implies that for

JCAP03(2026)035

any $J'_l \neq J_{l,\mathrm{obs}}$ (in practice in our case we used $J'_l = J_{l,\mathrm{obs}}(\mathcal{B})$ to compute results from a different set of J-factors as explained in section 3):

$$\mathcal{L}_{\mathrm{dSph},l}\left(\langle\sigma v\rangle; J'_l, \boldsymbol{\nu_l} \mid \boldsymbol{\mathcal{D}_l}\right) = \mathcal{L}_{\mathrm{dSph},l}\left(\frac{J'_l}{J_{l,\mathrm{obs}}}\langle\sigma v\rangle; J_{l,\mathrm{obs}}, \boldsymbol{\nu_l} \mid \boldsymbol{\mathcal{D}_l}\right), \tag{4.5}$$

which is a straightforward rescaling operation that reduces the computational needs of the profiling operation since:

$$\mathcal{L}\left(\langle\sigma v\rangle; \hat{\boldsymbol{\nu}} \mid \boldsymbol{\mathcal{D}}_{\mathrm{dSphs}}\right) = \prod_{l=1}^{N_{\mathrm{dSphs}}} \max_{J_l}\left[\mathcal{L}_{\mathrm{dSph},l}\left(\langle\sigma v\rangle; J_l, \hat{\boldsymbol{\nu}}_{\boldsymbol{l}} \mid \boldsymbol{\mathcal{D}_l}\right) \times \mathcal{J}_l\left(J_l \mid J_{l,\mathrm{obs}}, \sigma_{\log_{J_l}}\right)\right]. \tag{4.6}$$

In addition, eq. 4.5 enables the combination of data from different gamma-ray instruments and observed dSphs via tabulated values of $\mathcal{L}_{\mathrm{dSph},l}$ versus $\langle\sigma v\rangle$. In this work, we equivalently use tabulated values of λ from eq. 4.2 versus $\langle\sigma v\rangle$. The likelihood $\mathcal{L}_{\mathrm{dSph},l}$ is computed for a fixed value of J_l and profiled with respect to all instrumental nuisance parameters $\boldsymbol{\nu_l}$. These nuisance parameters are discussed in more detail below. These values are produced by each detector independently and therefore there is no need to share low-level information used to produce them, such as event lists or IRFs.

Figure 1 illustrates the multi-instrument combination technique used in this study with a comparison of the upper limit on $\langle\sigma v\rangle$ obtained from the combination of the observations of four experiments towards one dSph versus the upper limit from individual instruments. It also shows graphically the effect of the J-factor uncertainty on the combined observations.

The *partial* joint likelihood function for gamma-ray observations of each dSph ($\mathcal{L}_{\mathrm{dSph},l}$) is written as the product of the likelihood terms describing the $N_{\mathrm{exp},l}$ observations performed with any of our observatories:

$$\mathcal{L}_{\mathrm{dSph},l}\left(\langle\sigma v\rangle; J_l, \boldsymbol{\nu_l} \mid \boldsymbol{\mathcal{D}_l}\right) = \prod_{k=1}^{N_{\mathrm{exp},l}} \mathcal{L}_{lk}\left(\langle\sigma v\rangle; J_l, \boldsymbol{\nu_{lk}} \mid \boldsymbol{\mathcal{D}_{lk}}\right), \tag{4.7}$$

where each $\mathcal{L}_{lk}$ term refers to an observation of the l-th dSph with associated k-th IRFs. The quantity $N_{\mathrm{exp},l}$ varies from dSph to dSph and can be retrieved from table 1.

Each collaboration separately analyzes their data for $\boldsymbol{\mathcal{D}_{lk}}$ corresponding to dSph l and gamma-ray detector k, using as many common assumptions as possible in the analysis (see the next paragraph and further down in this section for additional details). We compute the values for the likelihood functions $\mathcal{L}_{lk}$ (see eq. 4.7) for a fixed value of J_l and profile over the rest of the nuisance parameters $\boldsymbol{\nu_{lk}}$. Then, values of λ from eq. 4.2 are computed as a function of $\langle\sigma v\rangle$ and shared using a common format. Results are computed for seven annihilation channels, W^+W^-, ZZ, $b\bar{b}$, $t\bar{t}$, e^+e^-, $\mu^+\mu^-$, and $\tau^+\tau^-$ over the 62 m_{DM} values between 5 GeV and 100 TeV provided in [51]. The $\langle\sigma v\rangle$ range is defined between 10^{-28} and $10^{-18}\mathrm{cm}^3 \cdot \mathrm{s}^{-1}$, with 1001 logarithmically spaced values. The likelihood combination, i.e. eq. 4.3, and profile over the J-factor to compute the profile likelihood ratio λ, i.e. eq. 4.2, are carried out with two different public analysis software packages, namely `gLike` [66] and `LklCom` [67], which provide the same results [68].

As mentioned previously, each experiment computes the $\mathcal{L}_{lk}$ from eq. 4.7 differently. The remainder of this section will describe the main differences between the approaches of each

JCAP03(2026)035

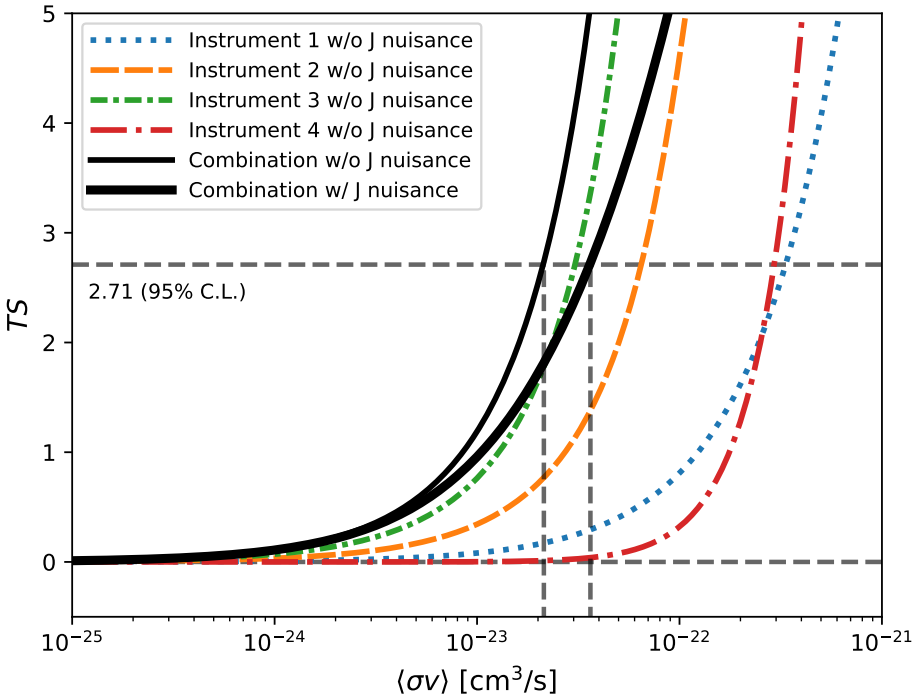

Figure 1. Illustration of a real data combination showing a comparison between TS provided by four instruments (non-solid colored lines) from the observation of the same dSph without any J-factor nuisance parameter included and their sum, i.e. the resulting combined likelihood (thin black line), for a DM particle mass of 20 TeV. The intersection of the likelihood profiles with the line TS = 2.71 indicates the 95% C.L. upper limit on $\langle\sigma v\rangle$ (see text for more details). The combined likelihood (thin black line) shows a smaller value of upper limit on $\langle\sigma v\rangle$ than those derived by individual instruments. We also show how the uncertainty on the J-factor affects the combined likelihood and degrades the upper limit on $\langle\sigma v\rangle$ (thick black line). All likelihood profiles are normalized so that the global minimum $\widehat{\langle\sigma v\rangle}$ is 0 to facilitate data handling. We note that each profile depends on the observational conditions under which a target object was observed. The sensitivity of a given instrument can be degraded and the upper limits less constraining if the observations suffer from non-optimal conditions such as a large zenith angle of observation or a short exposure time.

experiment. Four experiments, namely *Fermi*-LAT, HAWC, H.E.S.S. and MAGIC, use a binned likelihood to compute the $\mathcal{L}_{lk}$. VERITAS uses an unbinned likelihood approach described in detail at the end of this section. For the four experiments using a binned likelihood, for each observation $\boldsymbol{\mathcal{D}_{lk}}$ of a given dSph l carried out using a given gamma-ray detector k, the binned likelihood function is:

$$\begin{aligned}\mathcal{L}_{lk}\left(\langle\sigma v\rangle; J_l, \boldsymbol{\nu_{lk}} \mid \boldsymbol{\mathcal{D}_{lk}}\right) = \prod_{i=1}^{N_{\mathrm{E}'}} \prod_{j=1}^{N_{\mathrm{P}'}} \left[\mathcal{P}(s_{lk,ij}(\langle\sigma v\rangle, J_l, \boldsymbol{\nu_{lk}}) + b_{lk,ij}(\boldsymbol{\nu_{lk}}) \mid N_{lk,ij})\right] \\ \times \mathcal{L}_{lk,\boldsymbol{\nu}}\left(\boldsymbol{\nu_{lk}} \mid \boldsymbol{\mathcal{D}_{\nu_{lk}}}\right),\end{aligned} \tag{4.8}$$

where $N_{\mathrm{E}'}$ and $N_{\mathrm{P}'}$ are the number of considered bins in reconstructed energy and arrival direction, respectively. $\mathcal{P}$ represents a Poisson PDF for the number of gamma-ray candidate

JCAP03(2026)035

events $N_{lk,ij}$ observed in the i-th bin in energy and j-th bin in arrival direction, where the expected number is the sum of the expected mean number of signal events $s_{lk,ij}$ (produced by DM annihilation) and of background events $b_{lk,ij}$. $\mathcal{L}_{lk,\boldsymbol{\nu}}$ is the likelihood term for the extra $\boldsymbol{\nu_{lk}}$ nuisance parameters that vary from one instrument k to another. The expected counts for signal events s_{ij} for a given dSph l and detector k is given by:

$$s_{ij}(\langle\sigma v\rangle, J) = \int_{E'_{\mathrm{min},i}}^{E'_{\mathrm{max},i}} \mathrm{d}E' \int_{P'_{\mathrm{min},j}}^{P'_{\mathrm{max},j}} \mathrm{d}\Omega' \int_0^\infty \mathrm{d}E \int_{\Delta\Omega_{\mathrm{tot}}} \mathrm{d}\Omega \int_{t_{\mathrm{min}}}^{t_{\mathrm{max}}} \mathrm{d}t \frac{\mathrm{d}^2\Phi(\langle\sigma v\rangle, J)}{\mathrm{d}E\mathrm{d}\Omega} \times \mathrm{IRF}\left(E', P' \mid E, P, t\right), \tag{4.9}$$

where E' and E are the reconstructed and true energies, P' and P the reconstructed and true arrival directions; $E'_{\mathrm{min},i}$, $P'_{\mathrm{min},j}$, $E'_{\mathrm{max},i}$, and $P'_{\mathrm{max},j}$ are their lower and upper limits of the i-th energy bin and the j-th arrival direction bin; t_{min} and t_{max} delimit the time interval during which the dSph l was observed by the detector k; t is the time along the observations; $\mathrm{d}^2\Phi/\mathrm{d}E\mathrm{d}\Omega$ is the gamma-ray flux in the source region (see eq. 3.1); and $\mathrm{IRF}\left(E', P' \mid E, P, t\right)$ is the time-dependent IRF (IRF=0 in periods when there are no observations or during the detectors' deadtime). The IRF can be factored as the product of the effective collection area of the detector, $A_{\mathrm{eff}}(E, P, t)$, the PDF for the energy estimator, $f_E(E' \mid E, t)$, and the PDF for the arrival direction estimator, $f_P(P' \mid E, P, t)$: $\mathrm{IRF}(E', P' \mid E, P, t) = A_{\mathrm{eff}}(E, P, t) \times f_E(E' \mid E, t) \times f_P(P' \mid E, P, t)$. Note that for *Fermi*-LAT, HAWC, MAGIC, and VERITAS the effect of the finite angular resolution is taken into account through the convolution of $\mathrm{d}^2\Phi/\mathrm{d}E\mathrm{d}\Omega$ with f_P in eq. 4.9, whereas in the case of H.E.S.S., f_P is approximated by a delta function. This approximation has been made in order to maintain compatibility of the result with what has been previously published. The difference introduced by this approximation in the resulting s_{ij} is $< 5\%$ for all considered dSphs.

As mentioned above, the extra nuisance parameters designated by the $\mathcal{L}_{lk,\boldsymbol{\nu}}$ term in eq. 4.8 vary from one detector to another. One such difference is the treatment of the background. Analyses with *Fermi*-LAT and HAWC data model the background using a template fitting approach; therefore there is no $\mathcal{L}_{lk,\boldsymbol{\nu}}$ term in eq. 4.8 for either detector. On the other hand, IACTs (H.E.S.S., MAGIC, VERITAS) rely on ON/OFF measurements to estimate the background, which implies the use of an additional likelihood term $\mathcal{L}_{lk,\boldsymbol{\nu}}$ to describe this extra nuisance parameter. In practice, this additional likelihood corresponds to a Poisson term for the OFF observations $\mathcal{P}(\tau b \mid N_{\mathrm{OFF}})$, where N_{OFF} is the number of observed events in the OFF region, b is the number of expected background events, and the quantity τ is the acceptance-corrected exposure ratio between the ON and OFF regions. OFF regions are taken sufficiently far away from the signal region such that negligible DM signal is expected in the OFF regions.[4] This latter quantity, τ, is another nuisance parameter for this approach of background estimation and is therefore described by another likelihood term $\mathcal{T}$ including the statistical and systematic uncertainties on τ.

In this work, VERITAS uses a different likelihood than eq. 4.8 (see below for more details). Therefore, in practice, only H.E.S.S. and MAGIC use in their analysis the likelihood ($\mathcal{L}_{lk,\boldsymbol{\nu}}$)

[4]The DM halos of several targets (Carina, Draco, Fornax) are expected to be sufficiently extended that defining a signal-free background region is challenging. However, this leads to conservative estimation of the signal significance and the limits on the velocity-weighted annihilation cross section.

JCAP03(2026)035

with the extra nuisance parameters. In general, it is written as:

$$\mathcal{L}_{lk,\boldsymbol{\nu}}\left(\boldsymbol{\nu_{lk}} \mid \boldsymbol{\mathcal{D}_{\nu_{lk}}}\right) = \mathcal{P}(\tau b_{lk,ij} \mid N_{\mathrm{OFF},lk,ij}) \times \mathcal{T}\left(\tau \mid \tau_{\mathrm{obs}}, \sigma_\tau\right), \tag{4.10}$$

where $N_{\mathrm{OFF},lk,ij}$ and $b_{lk,ij}$ are respectively the number of observed events in the OFF region and the number of expected background events in the i-th bin of reconstructed energy and the j-th bin of reconstructed arrival direction. The PDF $\mathcal{T}$ for τ consists of a Gaussian function with mean τ_{obs} and standard deviation $\sigma_\tau = \sqrt{\sigma^2_{\tau,\mathrm{stat}} + \sigma^2_{\tau,\mathrm{syst}}}$, which includes statistical and systematic uncertainties, $\sigma_{\tau,\mathrm{stat}}$ and $\sigma_{\tau,\mathrm{syst}}$ respectively [41]. In practice, only the MAGIC analysis includes the treatment of τ as a nuisance parameter due to its deep exposure, and therefore high statistics, which implies the possibility of reaching the systematic ceiling of its sensitivity. In the analysis, MAGIC considers a systematic uncertainty of $\sigma_{\tau,\mathrm{syst}} = 0.015 \cdot \tau_{\mathrm{obs}}$ in the background estimation based on a dedicated performance study [39]. Note that the value of τ is the result of the profiling over the likelihood $\mathcal{T}$ and is always close to the mean value τ_{obs} computed as the ratio of the number of events in regions adjacent to the ON and OFF regions. H.E.S.S. finds this systematic effect to be negligible compared to the statistical uncertainties for their given datasets. We also note that eq. 4.10 and the above discussion concerns nuisance parameters related to the background estimate but there are other instrumental nuisance parameters. In particular, here we are overlooking uncertainties in the IRFs that may arise from discrepancies between the Monte Carlo simulations and the data.

Instead of the binned likelihood from eq. 4.8, VERITAS adopted an unbinned likelihood approach as described in [69], testing a null hypothesis (only background) against an alternative one (signal plus background hypothesis). The likelihood function is composed of the product of two Poisson probabilities in the ON and OFF regions, including the expected spectral shape information (known for a given DM model) in order to maximize the sensitivity to DM-originated gamma-ray signals. This likelihood function is defined in the following way:

$$\mathcal{L}_{lk}\left(\langle\sigma v\rangle; J_l, \boldsymbol{\nu_{lk}} \mid \boldsymbol{\mathcal{D}_{lk}}\right) = \frac{(s(\langle\sigma v\rangle, J_l) + b)^{N_{\mathrm{ON}}} e^{-(s(\langle\sigma v\rangle, J_l)+b)}}{N_{\mathrm{ON}}!} \frac{(\tau b)^{N_{\mathrm{OFF}}} e^{-\tau b}}{N_{\mathrm{OFF}}!} \prod_{i=1}^{N_{\mathrm{ON}}} P_i(E_i) \tag{4.11}$$

where N_{ON} and N_{OFF} are, respectively, the number of counts in the ON and OFF region, τ is the background normalization, b is the number of expected background events, P_i is the likelihood of the i-th event in the ON region to be reconstructed with measured energy E_i, and $s(\langle\sigma v\rangle, J_l)$ is the number of expected signal events. No extra nuisance parameters were considered in this unbinned likelihood approach; therefore there is no $\mathcal{L}_{lk,\boldsymbol{\nu}}$ term in eq. 4.11. Additionally, the VERITAS likelihood considers an energy-dependent point spread function with which the J-profile is convolved. To approximate the J-factor treatment of the other instruments, a single J-factor is used, derived from the energy-averaged convolved J-profile. Compared to the binned likelihood approach, the unbinned likelihood method used by VERITAS results in comparable limits. A more comprehensive review of the differences between the analyses of different instruments can be found in [70].

5 Results

No significant DM emission was detected with the combined analysis of data from the five instruments. We present the upper limits on $\langle\sigma v\rangle$ assuming seven independent DM self-

JCAP03(2026)035

annihilation channels, namely W^+W^-, ZZ, $b\bar{b}$, $t\bar{t}$, e^+e^-, $\mu^+\mu^-$, and $\tau^+\tau^-$. Our upper limits are determined by solving TS = 2.71, where 2.71 corresponds to a one-sided 95% confidence level assuming the test statistic behaves like a χ^2 distribution with one degree of freedom. This assumption is not entirely accurate because of the degeneracy between $\langle\sigma v\rangle$ and J in the gamma-ray flux computation (see eq. 3.1) and the fact that J is considered as a nuisance parameter with a log-normal PDF. Yet, using simulations we verified that solving TS = 2.71 produces an over-coverage and not an under-coverage. We therefore choose to compute upper limits using this definition as it is widely used, which allows easier comparison to previous results, and because over-coverage corresponds to more conservative limits.

The 68% and 95% containment bands are produced from 300 Poisson realizations of the null hypothesis corresponding to each of the combined datasets. These 300 realizations are combined identically to the data. The containment bands and the median are extracted from the distribution of resulting limits on the null hypothesis. These 300 realizations are obtained either by Poisson simulations of the OFF observations, for HAWC, H.E.S.S., MAGIC, and VERITAS, or taken from real observations of empty fields of view in the case of *Fermi*-LAT [19, 24, 25].

The obtained limits are shown in figure 2 for the $\mathcal{GS}$ set of J-factors [53] and in figure 3 for the $\mathcal{B}$ set of J-factors [52, 54]. The combined limits are presented with their 68% and 95% containment bands, and are expected to be close to the median limit when no signal is present. We observe agreement with the null hypothesis for all channels, within two standard deviations, between the observed limits and the expectations given by the median limits. Limits obtained from each detector are also indicated in the figures, where limits for all dSphs observed by the specific instrument have been combined.

Below $\sim$ 300 GeV, the limits obtained by *Fermi*-LAT dominate for all annihilation channels. From $\sim$ 300 GeV to $\sim$ 2 TeV, *Fermi*-LAT results continue to dominate for the hadronic ($b\bar{b}$ and $t\bar{t}$) and bosonic (W^+W^- and ZZ) DM channels, yet the IACTs (H.E.S.S., MAGIC, and VERITAS) and *Fermi*-LAT all contribute to the limit for leptonic (e^+e^-, $\mu^+\mu^-$, and $\tau^+\tau^-$) DM channels. For DM masses between $\sim$ 2 TeV and $\sim$ 10 TeV, the IACTs dominate leptonic DM annihilation channels, whereas both *Fermi*-LAT and the IACTs contribute strongly to the gauge boson and the quark DM annihilation channels. From $\sim$ 10 TeV to $\sim$ 100 TeV, both the IACTs and HAWC contribute significantly to the lepton annihilation channel limit. For the quark and gauge boson annihilation channels, the IACTs and *Fermi*-LAT both contribute strongly.

We note that there is a consistent and sizable under fluctuation at high masses in the limits we obtain in figure 3 with the $\mathcal{B}$ set of J-factors. It is due to the Ursa Major II dSph, whose J-factor increases by more than one order of magnitude compared to the $\mathcal{GS}$ set (see table 2), which makes it a dominant dSph for the combined limit. In particular in this range the MAGIC limit contributes significantly with 94.8 hours of observations while observing Ursa major II with a -2.1 σ excess. We further note that the limits computed using the $\mathcal{B}$ set of J-factors are always more constraining compared to the ones calculated with the $\mathcal{GS}$ set. For the W^+W^-, ZZ, $b\bar{b}$, and $t\bar{t}$ channels, the ratio between the limits computed with the two sets of J-factors varies by factors of 3–5 depending on the DM particle mass, with the largest ratio around 10 TeV. For the channels e^+e^-, $\mu^+\mu^-$, and $\tau^+\tau^-$, the ratio lies between

JCAP03(2026)035

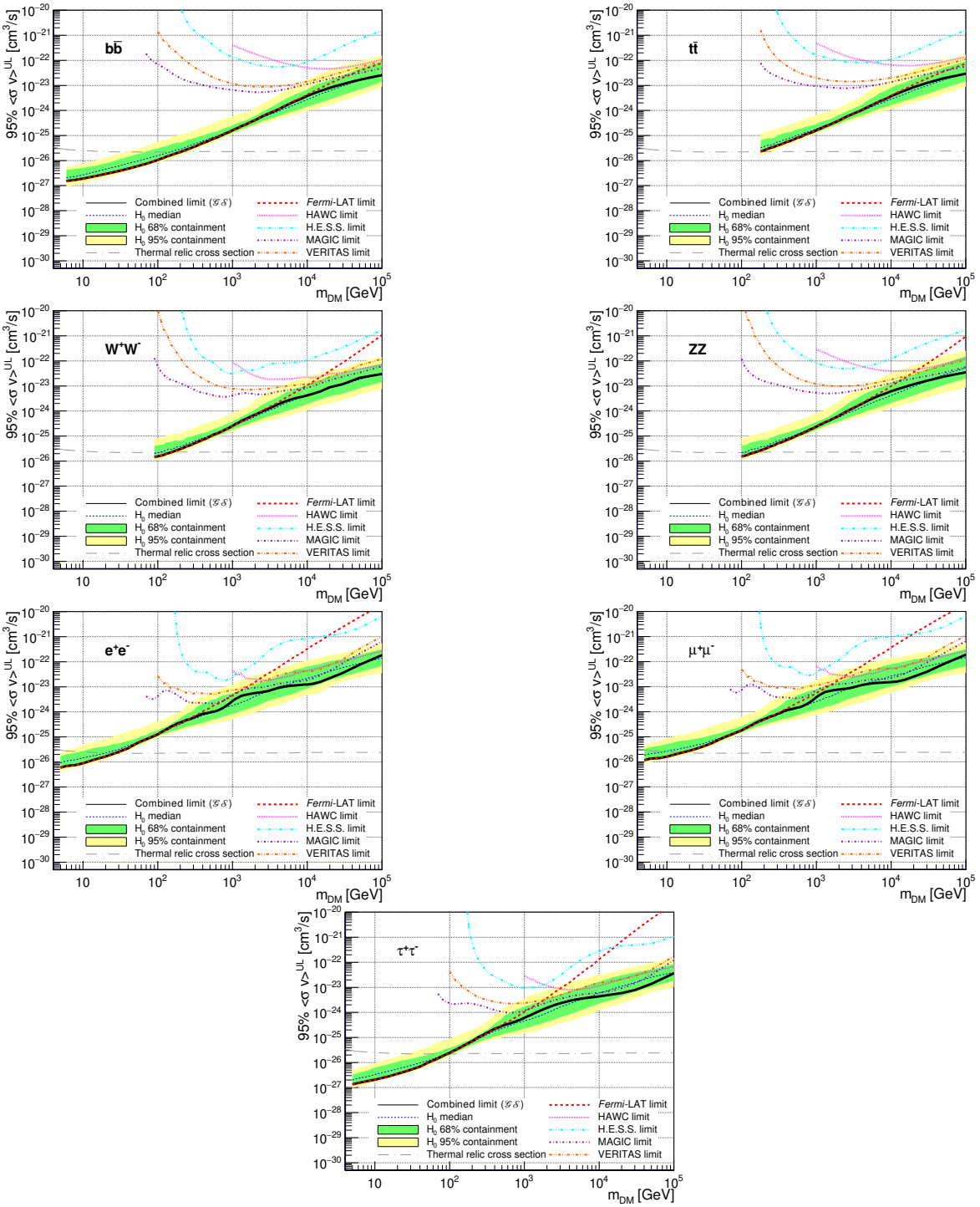

Figure 2. Upper limits at 95% confidence level on $\langle \sigma v \rangle$ as a function of the DM mass for seven annihilation channels, using the set of J-factors from [53] ($\mathcal{GS}$ set in table 2). The black solid line represents the observed combined limits obtained for the 20 dSphs included in this work, the blue dashed line is the median of the null hypothesis (H_0) corresponding to the expected limits with no DM signal ($\langle \sigma v \rangle = 0$), while the green and yellow bands show the 68% and 95% containment bands. Upper limits for each individual instrument are also indicated. The value of the thermal relic cross section as a function of the DM mass is given as the gray dotted-dashed line [9].

JCAP03(2026)035

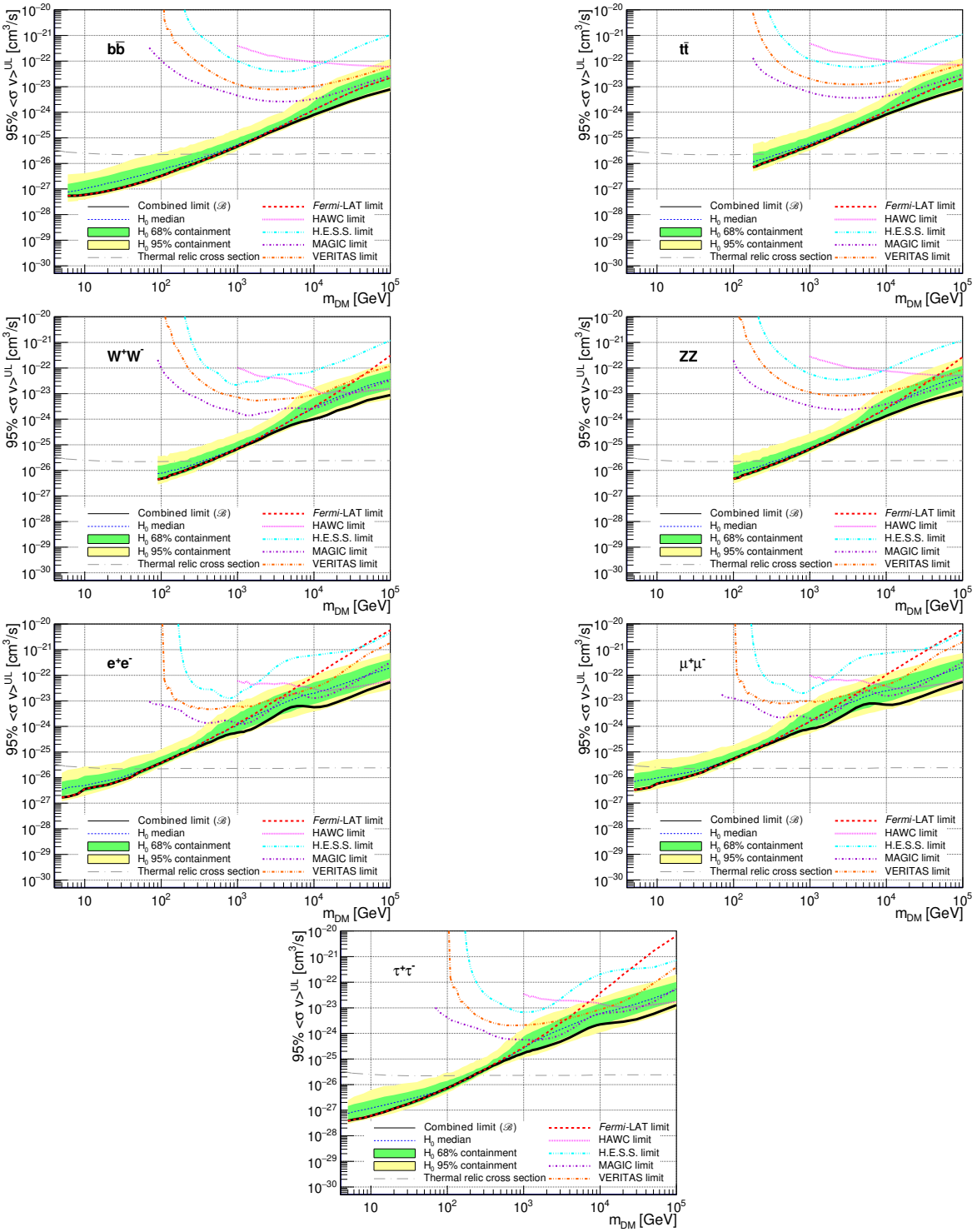

Figure 3. Same as figure 2, using the set of J-factors from [52, 54] ($\mathcal{B}$ set in table 2).

JCAP03(2026)035

2 and 6, peaking around 1 TeV. Examining figures 5 and 6 in appendix B, these differences are explained by the fact that the $\mathcal{B}$ set provides higher J-factors for the majority of the studied dSphs, with the notable exception of Segue 1 [56]. The variation on the ratio of the limits for the two sets is due to different dSphs dominating the limits at different DM particle masses. This comparison demonstrates the magnitude of systematic uncertainties associated with the choice of the J-factor calculation.

6 Discussion and conclusions

In this multi-instrument analysis, we used observations of 20 dSphs by the gamma-ray instruments *Fermi*-LAT, HAWC, H.E.S.S., MAGIC, and VERITAS to perform a collective search for DM annihilation signals. The data were combined across sources and detectors to increase the sensitivity of the search. We do not observe any significant deviation from the null hypothesis of no gamma-ray signal from DM. Therefore, we present our results in terms of upper limits on the thermally-averaged velocity-weighted annihilation cross section for seven potential DM annihilation channels.

Fermi-LAT data results in the most stringent constraints for all channels considered in this work for DM masses below approximately 1 TeV. The other telescopes contribute significantly at higher DM masses. Overall, for multi-TeV DM masses, the combined DM constraints from all five telescopes are 2–3 times stronger than for any individual telescope for multi-TeV DM, except for the hadronic channels, where the improvement of the combined analysis appears for DM masses above ~ 10 TeV. Similarly, a detected DM signal in the multi-TeV domain would have been 2–3 times more significant in this study than in any single-instrument search.

Assuming the DM content of the dSphs is relatively well constrained, our results produce robust limits derived from observations of various dSphs. Our combined analysis improves the sensitivity over previously published results from each individual detector and provides the most stringent limits on DM annihilation from dSphs. Our results are based on deep exposures of promising known dSphs with the most sensitive gamma-ray instruments currently in operation. The limits obtained span the largest mass range of any WIMP DM search. Therefore, we believe our results could constitute a legacy of a generation of gamma-ray instruments on WIMP DM searches towards dSphs. Nevertheless, these results can still be gradually improved as more data is collected, in particular from the large field of view instruments that are *Fermi*-LAT and HAWC for which the limits will decrease by at least one over the square root of total observation time, depending on the strength of the background and analysis approach [71]. Significant and more abrupt enhancements will require more sensitive instruments to be operational or new dSphs with significantly higher J-factors to be discovered.

While the limits shown extend to 100 TeV, the datasets used in this work are also suitable for setting limits on DM annihilation above 100 TeV, up to several PeV. However, a different input photon spectrum must be used in this mass range, reflecting the dominant particle physical processes at these energies [72], and the allowed theoretical benchmarks in this mass range differ from the simple thermal WIMP scenario. We limited ourselves to the mass range that has been previously studied by all instruments; so far only VERITAS has

JCAP03(2026)035

published limits in this mass range using the same data [58]. We leave a dedicated effort on the $> 100\,\mathrm{TeV}$ mass range for future work.

This analysis additionally serves as a proof of concept for future multi-instrument and multi-messenger combination analyses. With this collaborative effort, we have managed to sample over four orders in magnitude in gamma-ray energies with distinct observational techniques. Determining the nature of DM continues to be an elusive and difficult problem. Larger datasets with diverse measurement techniques can be essential in the DM search. Our collaborative work can be extended in the future to include other gamma-ray detectors such as LHAASO [73], CTA [74], and SWGO [75]. A future collaboration using similar techniques to the ones described in this paper could be applicable even beyond gamma rays. For example, the models we used for this study include annihilation channels with neutrinos in the final state. Advanced studies could aim to merge our results with those from neutrino observatories with large datasets such as IceCube [76], ANTARES [77], and KM3NeT [78]. Finally, an expansion of this analysis to include DM decay could also be considered.

Our analysis combines data from multiple instruments to produce strong constraints on astrophysical objects. From this perspective, these methods can be applied beyond DM searches. Almost every astrophysical study can benefit from multi-instrument, multi-wavelength gamma-ray studies, which make it possible to study the cosmos with greater precision and detail.

Acknowledgments

The *Fermi*-LAT Collaboration acknowledges generous ongoing support from a number of agencies and institutes that have supported both the development and the operation of the LAT as well as scientific data analysis. These include the National Aeronautics and Space Administration and the Department of Energy in the United States, the Commissariat à l'Energie Atomique and the Centre National de la Recherche Scientifique / Institut National de Physique Nucléaire et de Physique des Particules in France, the Agenzia Spaziale Italiana and the Istituto Nazionale di Fisica Nucleare in Italy, the Ministry of Education, Culture, Sports, Science and Technology (MEXT), High Energy Accelerator Research Organization (KEK) and Japan Aerospace Exploration Agency (JAXA) in Japan, and the K. A. Wallenberg Foundation, the Swedish Research Council and the Swedish National Space Board in Sweden. Additional support for science analysis during the operations phase is gratefully acknowledged from the Istituto Nazionale di Astrofisica in Italy and the Centre National d'Études Spatiales in France. This work performed in part under DOE Contract DE-AC02-76SF00515.

The HAWC collaboration acknowledges the support from: the US National Science Foundation (NSF); the US Department of Energy Office of High-Energy Physics; the Laboratory Directed Research and Development (LDRD) program of Los Alamos National Laboratory; Consejo Nacional de Ciencia y Tecnología (CONACyT), México, grants LNC-2023-117, 271051, 232656, 260378, 179588, 254964, 258865, 243290, 132197, A1-S-46288, A1-S-22784, CF-2023-I-645, cátedras 873, 1563, 341, 323, Red HAWC, México; DGAPA-UNAM grants IG101323, IN111716-3, IN111419, IA102019, IN106521, IN114924, IN110521, IN102223; VIEP-BUAP; PIFI 2012, 2013, PROFOCIE 2014, 2015; the University of Wisconsin Alumni Research Foundation; the Institute of Geophysics, Planetary Physics, and Signatures at Los Alamos

JCAP03(2026)035

National Laboratory; Polish Science Centre grant, 2024/53/B/ST9/02671; Coordinación de la Investigación Científica de la Universidad Michoacana; Royal Society — Newton Advanced Fellowship 180385; Gobierno de España and European Union — NextGenerationEU, grant CNS2023- 144099; The Program Management Unit for Human Resources & Institutional Development, Research and Innovation, NXPO (grant number B16F630069); Coordinación General Académica e Innovación (CGAI-UdeG), PRODEP-SEP UDG-CA-499; Institute of Cosmic Ray Research (ICRR), University of Tokyo. H.F. acknowledges support by NASA under award number 80GSFC21M0002. C.R. acknowledges support from National Research Foundation of Korea (RS-2023-00280210). We also acknowledge the significant contributions over many years of Stefan Westerhoff, Gaurang Yodh and Arnulfo Zepeda Domínguez, all deceased members of the HAWC collaboration. Thanks to Scott Delay, Luciano Díaz and Eduardo Murrieta for technical support.

The support of the Namibian authorities and of the University of Namibia in facilitating the construction and operation of H.E.S.S. is gratefully acknowledged, as is the support by the German Ministry for Education and Research (BMBF), the Max Planck Society, the German Research Foundation (DFG), the Helmholtz Association, the Alexander von Humboldt Foundation, the French Ministry of Higher Education, Research and Innovation, the Centre National de la Recherche Scientifique (CNRS/IN2P3 and CNRS/INSU), the Commissariat à l'énergie atomique et aux énergies alternatives (CEA), the U.K. Science and Technology Facilities Council (STFC), the Irish Research Council (IRC) and the Science Foundation Ireland (SFI), the Knut and Alice Wallenberg Foundation, the Polish Ministry of Education and Science, agreement no. 2021/WK/06, the South African Department of Science and Technology and National Research Foundation, the University of Namibia, the National Commission on Research, Science & Technology of Namibia (NCRST), the Austrian Federal Ministry of Education, Science and Research and the Austrian Science Fund (FWF), the Australian Research Council (ARC), the Japan Society for the Promotion of Science, the University of Amsterdam and the Science Committee of Armenia grant 21AG-1C085. We appreciate the excellent work of the technical support staff in Berlin, Zeuthen, Heidelberg, Palaiseau, Paris, Saclay, Tübingen and in Namibia in the construction and operation of the equipment. This work benefited from services provided by the H.E.S.S. Virtual Organisation, supported by the national resource providers of the EGI Federation.

The MAGIC collaboration would like to thank the Instituto de Astrofísica de Canarias for the excellent working conditions at the Observatorio del Roque de los Muchachos in La Palma. The financial support of the German BMBF, MPG and HGF; the Italian INFN and INAF; the Swiss National Fund SNF; the grants PID2019-104114RB-C31, PID2019-104114RB-C32, PID2019-104114RB-C33, PID2019-105510GB-C31, PID2019-107847RB-C41, PID2019-107847RB-C42, PID2019-107847RB-C44, PID2019-107988GB-C22, PID2022-136828NB-C41, PID2022-137810NB-C22, PID2022-138172NB-C41, PID2022-138172NB-C42, PID2022-138172NB-C43, PID2022-139117NB-C41, PID2022-139117NB-C42, PID2022-139117NB-C43, PID2022-139117NB-C44 funded by the Spanish MCIN/AEI/ 10.13039/501100011033 and "ERDF A way of making Europe"; the Indian Department of Atomic Energy; the Japanese ICRR, the University of Tokyo, JSPS, and MEXT; the Bulgarian Ministry of Education and Science, National RI Roadmap Project DO1-400/18.12.2020 and the Academy of Finland grant

JCAP03(2026)035

nr. 320045 is gratefully acknowledged. This work was also been supported by Centros de Excelencia “Severo Ochoa” y Unidades “María de Maeztu” program of the Spanish MCIN/AEI/10.13039/501100011033 (CEX2019-000920-S, CEX2019-000918-M, CEX2021-001131-S) and by the CERCA institution and grants 2021SGR00426 and 2021SGR00773 of the Generalitat de Catalunya; by the Croatian Science Foundation (HrZZ) Project IP-2022-10-4595 and the University of Rijeka Project uniri-prirod-18-48; by the Deutsche Forschungsgemeinschaft (SFB1491) and by the Lamarr-Institute for Machine Learning and Artificial Intelligence; by the Polish Ministry Of Education and Science grant No. 2021/WK/08; and by the Brazilian MCTIC, CNPq and FAPERJ. This work was supported by the Grant RYC2021-032552-I funded by MCIN/AEI/10.13039/501100011033 and by the European Union NextGenerationEU/PRTR.

The research of VERITAS is supported by grants from the U.S. Department of Energy Office of Science, the U.S. National Science Foundation and the Smithsonian Institution, by NSERC in Canada, and by the Helmholtz Association (including the Young Investigators Program of the Helmholtz Association) in Germany. This research used resources provided by the Open Science Grid, which is supported by the National Science Foundation and the U.S. Department of Energy’s Office of Science, and resources of the National Energy Research Scientific Computing Center (NERSC), a U.S. Department of Energy Office of Science User Facility operated under Contract No. DE-AC02-05CH11231. We acknowledge the excellent work of the technical support staff at the Fred Lawrence Whipple Observatory and at the collaborating institutions in the construction and operation of the instrument.

JCAP03(2026)035

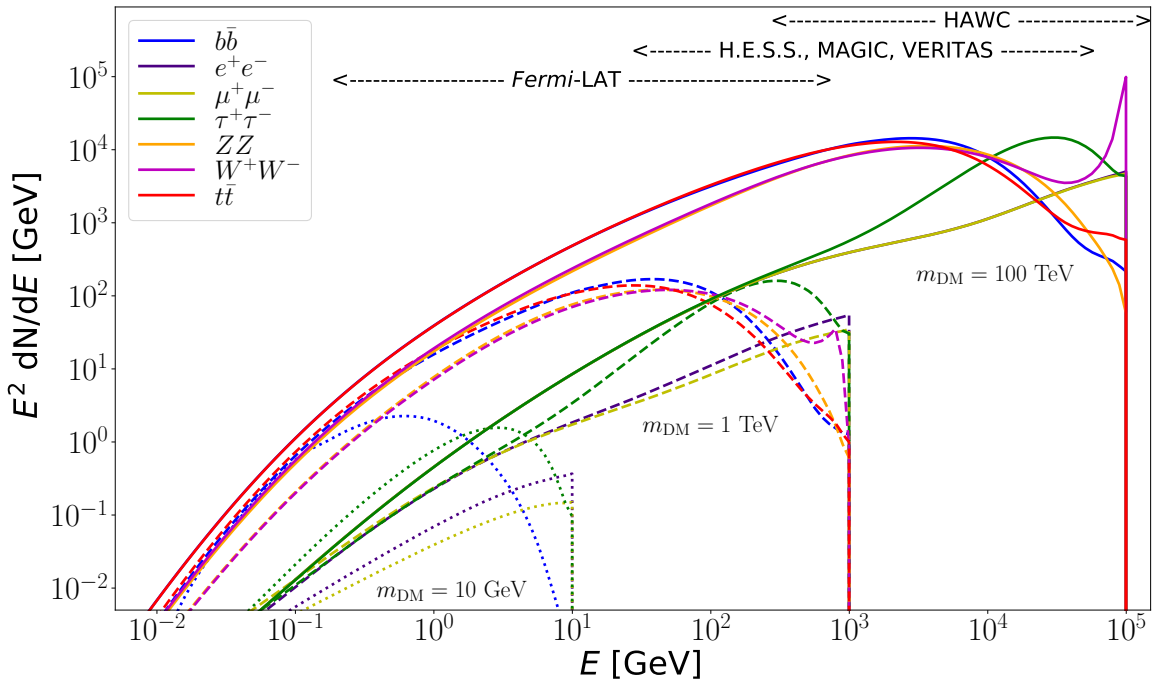

Figure 4. Differential photon yield per DM annihilation into SM pairs $b\bar{b}$ (blue), e^+e^- (indigo), $\mu^+\mu^-$ (light green), $\tau^+\tau^-$ (dark green), ZZ (orange), W^+W^- (magenta), and $t\bar{t}$ (red) for DM masses of 10 GeV (dotted), 1 TeV (dashed), and 100 TeV (solid). The approximate energy ranges of the gamma-ray instruments using in this work (see section 2) are depicted at the top of the figure.

A dN/dE spectra

We show in this appendix the differential photon yield per DM annihilation in figure 4, as computed by Cirelli et al. [51]. The computation of the photon yield includes electroweak corrections of the final state products.

B *J*-factor distributions

We show in this appendix a comparison between the J-factors computed by Geringer-Sameth et al. [53] (the $\mathcal{GS}$ set) and the ones computed by Bonnivard et al. [52, 54] (the $\mathcal{B}$ set).

The $\mathcal{GS}$ J-factors are computed through a Jeans analysis of the kinematic stellar data of the selected dSphs, assuming a dynamic equilibrium and a spherical symmetry for the dSphs. In [53] the authors adopted the generalized DM density distribution, known as Zhao-Hernquist and introduced in [79], which carries three additional index parameters to describe the inner and outer slopes, and the break of the density profile. Such a profile parametrization allows the reduction of the theoretical bias from the choice of a specific radial dependency on the kinematic data. In addition, a constant velocity anisotropy profile and a Plummer light profile [80] for the stellar distribution were assumed. The velocity anisotropy profile depends on the radial and tangential velocity dispersions. However, its determination remains challenging since only the line-of-sight velocity dispersion can be

JCAP03(2026)035

derived from velocity measurements. Therefore, the parametrization of the anisotropy profile is obtained from simulated halos (see [81] for more details).

The $\mathcal{B}$ J-factors were computed through a Jeans analysis taking into account the systematic uncertainties induced by the DM profile parametrization, the radial velocity anisotropy profile, and the triaxiality of the halo of the dSphs. In [52, 54] the authors performed a study relying on different modelling choices and treatment of systematic uncertainties than $\mathcal{GS}$ for the determination of the J-factor. Conservative values of the J-factors were obtained using an Einasto DM density profile [82], a realistic anisotropy profile known as the Baes & Van Hese profile [83] which takes into account that the inner regions can be significantly non-isotropic, and a Zhao-Hernquist light profile [79] to fit the distribution of the luminous matter.

For both sets, J-factor values are provided for all dSphs as a function of the radius of the integration region [52–54]. Table 2 shows the heliocentric distance and Galactic coordinates of the 20 dSphs, together with the two sets of J-factor values integrated up to the outermost observed star for $\mathcal{GS}$ and the tidal radius for $\mathcal{B}$. Both J-factor sets were derived through a Jeans analysis based on the same kinematic data, except for Draco, where the measurements of [84] have been adopted in the computation of the $\mathcal{B}$ value. The computations for producing the $\mathcal{GS}$ and $\mathcal{B}$ samples differ in the choice of the DM density, velocity anisotropy, and light profiles, for which the set $\mathcal{B}$ takes into account some sources of systematic uncertainties.

Figures 5 and 6 show the comparisons of the J-factor versus the angular radius for each of the 20 dSphs used in this study. The uncertainties provided by the authors are also indicated in the figures. As for table 2, for the $\mathcal{GS}$ set, the computation stops at the angular radius corresponding to the outermost observed star, while for the $\mathcal{B}$ set, the computation stops at the angular radius corresponding to the tidal radius. These J-factors are then translated into spatial templates for each experiment using the instrument point spread function. Note that the integral over $\Delta\Omega$ in eq. 4.9 requires knowing the value of $\mathrm{d}J/\mathrm{d}\Omega$ for angular distance covering the whole DM halo, which is not the case in general for the $\mathcal{GS}$ sample as can be seen in figures 5 and 6. This does not affect the computation for Cherenkov telescopes, since for all their observed dSph $\mathcal{GS}$ covers a range of angular distance above the size of the signal integration region. HAWC considers $\mathrm{d}J/\mathrm{d}\Omega = 0$ for angular distances above the maximum ones provided by $\mathcal{GS}$, thus producing conservative upper limits on $\langle\sigma v\rangle$. Finally, *Fermi*-LAT has assumed the DM template to be point-like as for most of the dSphs the extension of the DM halos is smaller than the LAT PSF [85]. Ref. [86] investigated the effect of including the spatial extension of the DM template in the analysis, which could weaken the *Fermi*-LAT upper limits by at most a factor $1.5 - 1.8$ depending on the annihilation channel.

JCAP03(2026)035

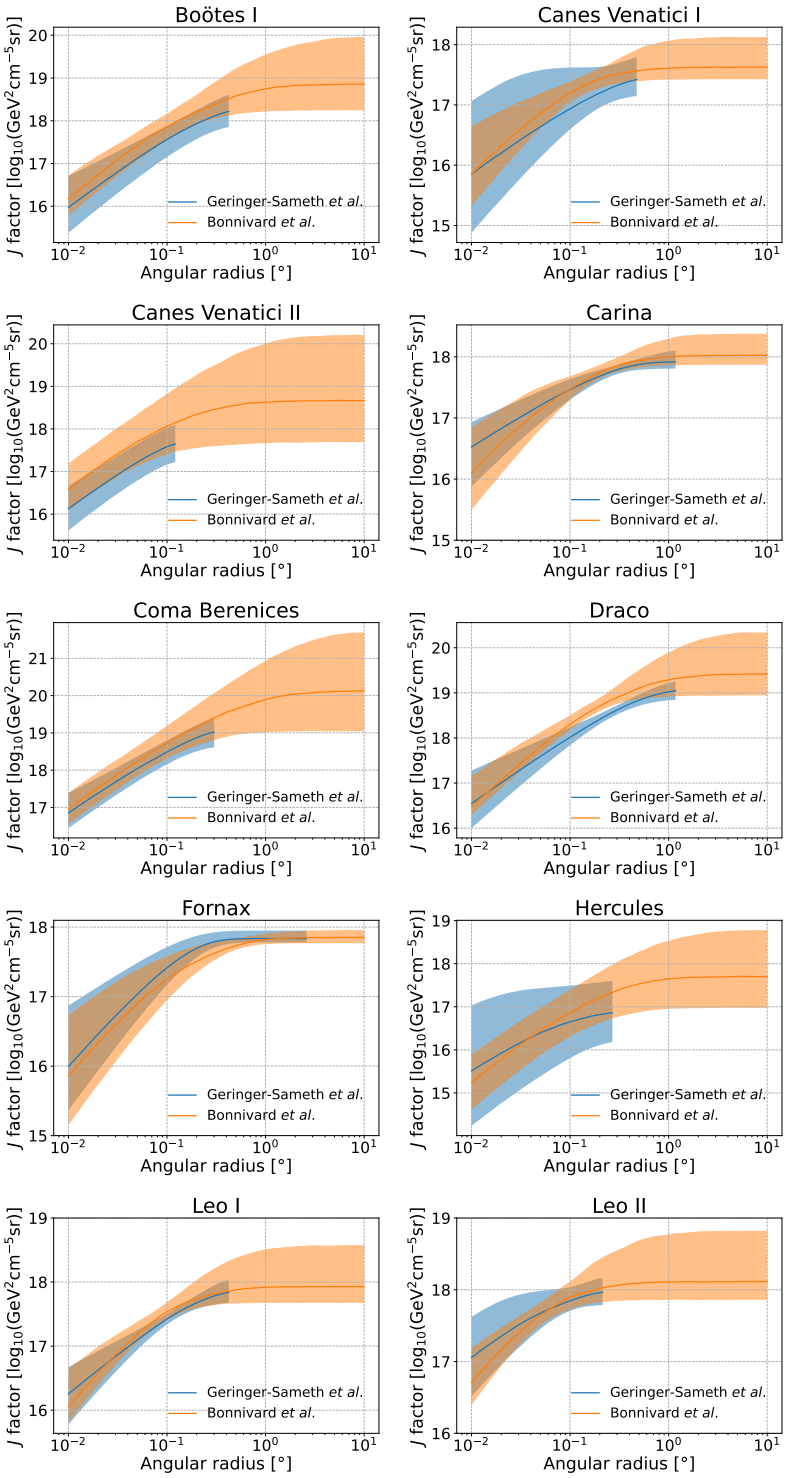

Figure 5. Comparisons between the J-factors used for this study versus the angular radius. Computed J-factors from [53] ($\mathcal{GS}$ set in table 2) are extended up to the outermost visible star and are in blue. The J-factors computed from [52, 54] ($\mathcal{B}$ set in table 2) are extended up to the tidal radius of the dwarfs and are in orange. The solid lines represent the most probable value of the J-factors while the shaded regions correspond to the 1σ standard deviation.

JCAP03(2026)035

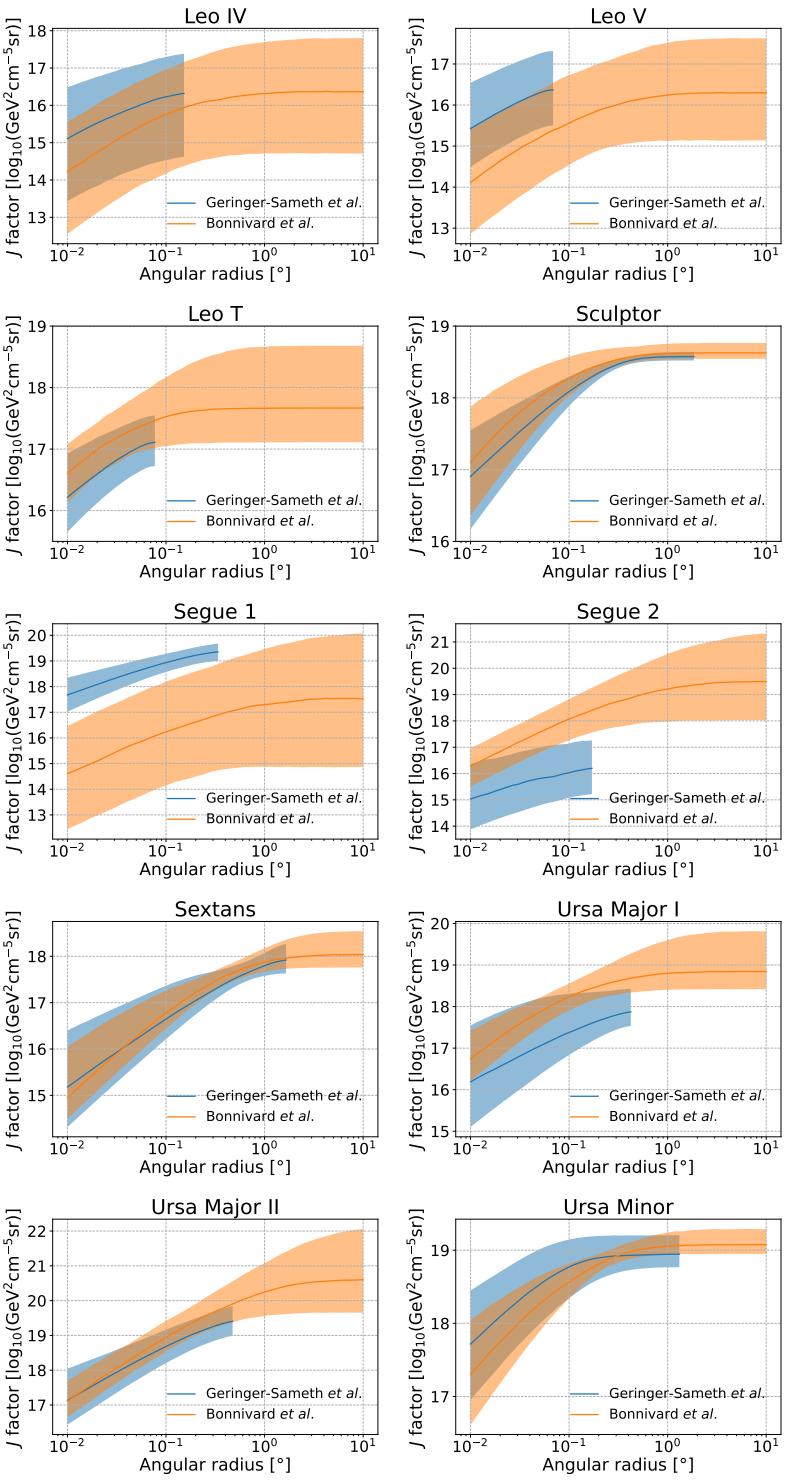

Figure 6. Continuation of figure 5.

JCAP03(2026)035

References

[1] Planck collaboration, *Planck 2018 results. VI. Cosmological parameters*, *Astron. Astrophys.* **641** (2020) A6 [*Erratum ibid.* **652** (2021) C4] [arXiv:1807.06209] [inSPIRE].

[2] S. Schuldt et al., *Inner dark matter distribution of the Cosmic Horseshoe (J1148+1930) with gravitational lensing and dynamics*, *Astron. Astrophys.* **631** (2019) A40 [arXiv:1901.02896] [inSPIRE].

[3] V. Springel, C.S. Frenk and S.D.M. White, *The large-scale structure of the universe*, *Nature* **440** (2006) 1137 [astro-ph/0604561] [inSPIRE].

[4] Planck collaboration, *Planck 2015 results. XIII. Cosmological parameters*, *Astron. Astrophys.* **594** (2016) A13 [arXiv:1502.01589] [inSPIRE].

[5] T.S. van Albada, J.N. Bahcall, K. Begeman and R. Sancisi, *The distribution of dark matter in the spiral galaxy NGC-3198*, *Astrophys. J.* **295** (1985) 305 [inSPIRE].

[6] L. Roszkowski, E.M. Sessolo and S. Trojanowski, *WIMP dark matter candidates and searches — current status and future prospects*, *Rept. Prog. Phys.* **81** (2018) 066201 [arXiv:1707.06277] [inSPIRE].

[7] A. De Angelis and M. Pimenta, *Introduction to particle and astroparticle physics: multimessenger astronomy and its particle physics foundations*, Springer Nature, Heidelberg, Germany (2018) [DOI:10.1007/978-3-319-78181-5] [inSPIRE].

[8] P. Salati, *Dark matter annihilation in the universe*, *Int. J. Mod. Phys. Conf. Ser.* **30** (2014) 1460256 [arXiv:1403.4495] [inSPIRE].

[9] G. Steigman, B. Dasgupta and J.F. Beacom, *Precise relic WIMP abundance and its impact on searches for dark matter annihilation*, *Phys. Rev. D* **86** (2012) 023506 [arXiv:1204.3622] [inSPIRE].

[10] L.E. Strigari, *Dark matter in dwarf spheroidal galaxies and indirect detection: a review*, *Rept. Prog. Phys.* **81** (2018) 056901 [arXiv:1805.05883] [inSPIRE].

[11] J. Binney and M. Merrifield, *Galactic astronomy*, Princeton University Press, Princeton, NJ, U.S.A. (1998).

[12] J. Binney and S. Tremaine, *Galactic dynamics*, second edition, Princeton University Press, Princeton, NJ, U.S.A. (2008).

[13] K. Spekkens et al., *The dearth of neutral hydrogen in galactic dwarf spheroidal galaxies*, *Astrophys. J.* **795** (2014) L5 [arXiv:1410.0028].

[14] N.W. Evans, F. Ferrer and S. Sarkar, *A 'Baedecker' for the dark matter annihilation signal*, *Phys. Rev. D* **69** (2004) 123501 [astro-ph/0311145] [inSPIRE].

[15] M. Winter, G. Zaharijas, K. Bechtol and J. Vandenbroucke, *Estimating the GeV emission of millisecond pulsars in dwarf spheroidal galaxies*, *Astrophys. J. Lett.* **832** (2016) L6 [arXiv:1607.06390] [inSPIRE].

[16] MAGIC and Fermi-LAT collaborations, *Limits to dark matter annihilation cross-section from a combined analysis of MAGIC and Fermi-LAT observations of dwarf satellite galaxies*, *JCAP* **02** (2016) 039 [arXiv:1601.06590] [inSPIRE].

[17] Fermi-LAT collaboration, *The Large Area Telescope on the Fermi gamma-ray space telescope mission*, *Astrophys. J.* **697** (2009) 1071 [arXiv:0902.1089] [inSPIRE].

JCAP03(2026)035

[18] Fermi-LAT collaboration, *The Fermi Large Area Telescope on orbit: event classification, instrument response functions, and calibration*, *Astrophys. J. Suppl.* **203** (2012) 4 [arXiv:1206.1896] [INSPIRE].

[19] Fermi-LAT collaboration, *Searching for dark matter annihilation from Milky Way dwarf spheroidal galaxies with six years of Fermi Large Area Telescope data*, *Phys. Rev. Lett.* **115** (2015) 231301 [arXiv:1503.02641] [INSPIRE].

[20] Fermi-LAT collaboration, *Pass 8: toward the full realization of the Fermi-LAT scientific potential*, arXiv:1303.3514 [INSPIRE].

[21] Fermi-LAT collaboration, *Fermi-LAT improved Pass 8 event selection*, in the proceedings of the *8th international Fermi symposium: celebrating 10 year of Fermi*, (2018) [arXiv:1810.11394] [INSPIRE].

[22] Fermi-LAT collaboration, *Updated search for spectral lines from Galactic dark matter interactions with pass 8 data from the Fermi Large Area Telescope*, *Phys. Rev. D* **91** (2015) 122002 [arXiv:1506.00013] [INSPIRE].

[23] Fermi-LAT collaboration, *Fermi Large Area Telescope fourth source catalog*, *Astrophys. J. Suppl.* **247** (2020) 33 [arXiv:1902.10045] [INSPIRE].

[24] Fermi-LAT and DES collaborations, *Searching for dark matter annihilation in recently discovered Milky Way satellites with Fermi-LAT*, *Astrophys. J.* **834** (2017) 110 [arXiv:1611.03184] [INSPIRE].

[25] M. Di Mauro and M.W. Winkler, *Multimessenger constraints on the dark matter interpretation of the Fermi-LAT galactic center excess*, *Phys. Rev. D* **103** (2021) 123005 [arXiv:2101.11027] [INSPIRE].

[26] HAWC collaboration, *3HWC: the third HAWC catalog of very-high-energy gamma-ray sources*, *Astrophys. J.* **905** (2020) 76 [arXiv:2007.08582] [INSPIRE].

[27] A.U. Abeysekara et al., *Observation of the Crab nebula with the HAWC gamma-ray observatory*, *Astrophys. J.* **843** (2017) 39 [arXiv:1701.01778] [INSPIRE].

[28] G. Vianello et al., *The Multi-Mission Maximum Likelihood framework (3ML)*, arXiv:1507.08343 [INSPIRE].

[29] HAWC collaboration, *Dark matter limits from dwarf spheroidal galaxies with the HAWC gamma-ray observatory*, *Astrophys. J.* **853** (2018) 154 [arXiv:1706.01277] [INSPIRE].

[30] V.P. Fomin et al., *New methods of atmospheric Cherenkov imaging for gamma-ray astronomy. 1: the false source method*, *Astropart. Phys.* **2** (1994) 137 [INSPIRE].

[31] H.E.S.S. collaboration, *Observations of the Crab nebula with H.E.S.S.*, *Astron. Astrophys.* **457** (2006) 899 [astro-ph/0607333] [INSPIRE].

[32] M. de Naurois and L. Rolland, *A high performance likelihood reconstruction of gamma-rays for imaging atmospheric Cherenkov telescopes*, *Astropart. Phys.* **32** (2009) 231 [arXiv:0907.2610] [INSPIRE].

[33] D. Berge, S. Funk and J. Hinton, *Background modelling in very-high-energy gamma-ray astronomy*, *Astron. Astrophys.* **466** (2007) 1219 [astro-ph/0610959] [INSPIRE].

[34] T.-P. Li and Y.-Q. Ma, *Analysis methods for results in gamma-ray astronomy*, *Astrophys. J.* **272** (1983) 317 [INSPIRE].

[35] H.E.S.S. collaboration, *H.E.S.S. constraints on dark matter annihilations towards the Sculptor and Carina dwarf galaxies*, *Astropart. Phys.* **34** (2011) 608 [arXiv:1012.5602] [INSPIRE].

JCAP03(2026)035

[36] H.E.S.S. collaboration, *Search for dark matter annihilation signatures in H.E.S.S. observations of dwarf spheroidal galaxies*, *Phys. Rev. D* **90** (2014) 112012 [arXiv:1410.2589] [INSPIRE].

[37] HESS collaboration, *Searches for gamma-ray lines and 'pure WIMP' spectra from dark matter annihilations in dwarf galaxies with H.E.S.S.*, *JCAP* **11** (2018) 037 [arXiv:1810.00995] [INSPIRE].

[38] R.D. Parsons and J.A. Hinton, *A Monte Carlo template based analysis for air-Cherenkov arrays*, *Astropart. Phys.* **56** (2014) 26 [arXiv:1403.2993] [INSPIRE].

[39] MAGIC collaboration, *The major upgrade of the MAGIC telescopes, part II: a performance study using observations of the Crab nebula*, *Astropart. Phys.* **72** (2016) 76 [arXiv:1409.5594] [INSPIRE].

[40] J. Aleksić et al., *Optimized dark matter searches in deep observations of Segue 1 with MAGIC*, *JCAP* **02** (2014) 008 [arXiv:1312.1535] [INSPIRE].

[41] MAGIC collaboration, *Indirect dark matter searches in the dwarf satellite galaxy Ursa Major II with the MAGIC telescopes*, *JCAP* **03** (2018) 009 [arXiv:1712.03095] [INSPIRE].

[42] MAGIC collaboration, *Combined searches for dark matter in dwarf spheroidal galaxies observed with the MAGIC telescopes, including new data from Coma Berenices and Draco*, *Phys. Dark Univ.* **35** (2022) 100912 [arXiv:2111.15009] [INSPIRE].

[43] J. Aleksić et al., *The major upgrade of the MAGIC telescopes, part I: the hardware improvements and the commissioning of the system*, *Astropart. Phys.* **72** (2016) 61 [arXiv:1409.6073] [INSPIRE].

[44] A. Moralejo et al., *MARS, the MAGIC Analysis and Reconstruction Software*, in *International Cosmic Ray Conference*, volume 33, January 2013, p. 2937 [arXiv:0907.0943].

[45] VERITAS collaboration, *Performance of the VERITAS experiment*, *PoS* **ICRC2015** (2016) 771 [arXiv:1508.07070] [INSPIRE].

[46] VERITAS collaboration, *Dark matter constraints from a joint analysis of dwarf spheroidal galaxy observations with VERITAS*, *Phys. Rev. D* **95** (2017) 082001 [arXiv:1703.04937] [INSPIRE].

[47] VERITAS collaboration, *Dark matter annihilation limits from dwarf galaxies using VERITAS*, in the proceedings of the *33rd International Cosmic Ray Conference*, (2013) [arXiv:1307.8367] [INSPIRE].

[48] G.P. Rowell, *A new template background estimate for source searching in TeV gamma-ray astronomy*, *Astron. Astrophys.* **410** (2003) 389 [astro-ph/0310025] [INSPIRE].

[49] VERITAS collaboration, *VEGAS, the VERITAS Gamma-ray Analysis Suite*, arXiv:0709.4233 [INSPIRE].

[50] G. Bertone, D. Hooper and J. Silk, *Particle dark matter: evidence, candidates and constraints*, *Phys. Rept.* **405** (2005) 279 [hep-ph/0404175] [INSPIRE].

[51] M. Cirelli et al., *PPPC 4 DM ID: a Poor Particle Physicist Cookbook for Dark Matter Indirect Detection*, *JCAP* **03** (2011) 051 [*Erratum ibid.* **10** (2012) E01] [arXiv:1012.4515] [INSPIRE].

[52] V. Bonnivard, C. Combet, D. Maurin and M.G. Walker, *Spherical Jeans analysis for dark matter indirect detection in dwarf spheroidal galaxies — impact of physical parameters and triaxiality*, *Mon. Not. Roy. Astron. Soc.* **446** (2015) 3002 [arXiv:1407.7822] [INSPIRE].

JCAP03(2026)035

[53] A. Geringer-Sameth, S.M. Koushiappas and M. Walker, *Dwarf galaxy annihilation and decay emission profiles for dark matter experiments*, *Astrophys. J.* **801** (2015) 74 [arXiv:1408.0002] [INSPIRE].

[54] V. Bonnivard et al., *Dark matter annihilation and decay in dwarf spheroidal galaxies: the classical and ultrafaint dSphs*, *Mon. Not. Roy. Astron. Soc.* **453** (2015) 849 [arXiv:1504.02048] [INSPIRE].

[55] K.K. Boddy et al., *Effective J-factors for Milky Way dwarf spheroidal galaxies with velocity-dependent annihilation*, *Phys. Rev. D* **102** (2020) 023029 [arXiv:1909.13197] [INSPIRE].

[56] V. Bonnivard, D. Maurin and M.G. Walker, *Contamination of stellar-kinematic samples and uncertainty about dark matter annihilation profiles in ultrafaint dwarf galaxies: the example of Segue I*, *Mon. Not. Roy. Astron. Soc.* **462** (2016) 223 [arXiv:1506.08209] [INSPIRE].

[57] S. Ando et al., *Structure formation models weaken limits on WIMP dark matter from dwarf spheroidal galaxies*, *Phys. Rev. D* **102** (2020) 061302 [arXiv:2002.11956] [INSPIRE].

[58] VERITAS collaboration, *Indirect search for dark matter with a combined analysis of dwarf spheroidal galaxies from VERITAS*, *Phys. Rev. D* **110** (2024) 063034 [arXiv:2407.16518] [INSPIRE].

[59] H.E.S.S. collaboration, *Observations of the Sagittarius dwarf galaxy by the H.E.S.S. experiment and search for a dark matter signal*, *Astropart. Phys.* **29** (2008) 55 [*Erratum ibid.* **33** (2010) 274] [arXiv:0711.2369] [INSPIRE].

[60] A. Viana et al., *Prospects for a dark matter annihilation signal toward the Sagittarius dwarf galaxy with ground-based Cherenkov telescopes*, *Astrophys. J.* **746** (2012) 77 [arXiv:1103.2627] [INSPIRE].

[61] H.E.S.S. collaboration, *Search for dark matter signals towards a selection of recently detected DES dwarf galaxy satellites of the Milky Way with H.E.S.S.*, *Phys. Rev. D* **102** (2020) 062001 [arXiv:2008.00688] [INSPIRE].

[62] MAGIC collaboration, *A search for dark matter in Triangulum II with the MAGIC telescopes*, *Phys. Dark Univ.* **28** (2020) 100529 [arXiv:2003.05260] [INSPIRE].

[63] E.N. Kirby, J.G. Cohen, J.D. Simon and P. Guhathakurta, *Triangulum II: possibly a very dense ultra-faint dwarf galaxy*, *Astrophys. J. Lett.* **814** (2015) L7 [arXiv:1510.03856] [INSPIRE].

[64] J.L. Carlin et al., *Deep Subaru Hyper Suprime-Cam observations of Milky Way satellites Columba I and Triangulum II*, *Astron. J.* **154** (2017) 267 [arXiv:1710.06444] [INSPIRE].

[65] G. Cowan, K. Cranmer, E. Gross and O. Vitells, *Asymptotic formulae for likelihood-based tests of new physics*, *Eur. Phys. J. C* **71** (2011) 1554 [*Erratum ibid.* **73** (2013) 2501] [arXiv:1007.1727] [INSPIRE].

[66] J. Rico, C. Nigro, D. Kerszberg and T. Miener, *glike: numerical maximization of heterogeneous joint likelihood functions of a common free parameter plus nuisance parameters*, Zenodo, November 2022.

[67] T. Miener and D. Nieto, *Lklcom: combining likelihoods from different experiments*, Zenodo, March 2021.

[68] T. Miener et al., *Open-source analysis tools for multi-instrument dark matter searches*, *ASP Conf. Ser.* **535** (2024) 17 [arXiv:2112.01818] [INSPIRE].

[69] VERITAS collaboration, *The VERITAS dark matter program*, *PoS* **ICRC2017** (2018) 904 [arXiv:1708.07447] [INSPIRE].

JCAP03(2026)035

[70] J. Rico, *Gamma-ray dark matter searches in Milky Way satellites — a comparative review of data analysis methods and current results*, *Galaxies* **8** (2020) 25 [arXiv:2003.13482] [INSPIRE].

[71] A. McDaniel et al., *Legacy analysis of dark matter annihilation from the Milky Way dwarf spheroidal galaxies with 14 years of Fermi-LAT data*, *Phys. Rev. D* **109** (2024) 063024 [arXiv:2311.04982] [INSPIRE].

[72] C.W. Bauer, N.L. Rodd and B.R. Webber, *Dark matter spectra from the electroweak to the Planck scale*, *JHEP* **06** (2021) 121 [arXiv:2007.15001] [INSPIRE].

[73] F. Aharonian et al., *The observation of the Crab nebula with LHAASO-KM2A for the performance study*, *Chin. Phys. C* **45** (2021) 025002 [arXiv:2010.06205] [INSPIRE].

[74] CTA CONSORTIUM collaboration, *Science with the Cherenkov Telescope Array*, World Scientific, Singapore (2018) [DOI:10.1142/10986] [INSPIRE].

[75] P. Abreu et al., *The Southern Wide-Field Gamma-Ray Observatory (SWGO): a next-generation ground-based survey instrument for VHE gamma-ray astronomy*, *Bull. Amer. Astron. Soc.* **51** (2019) 109 [arXiv:1907.07737] [INSPIRE].

[76] ICECUBE collaboration, *The IceCube neutrino observatory: instrumentation and online systems*, 2017 *JINST* **12** P03012 [*Erratum ibid.* **19** (2024) E05001] [arXiv:1612.05093] [INSPIRE].

[77] ANTARES collaboration, *ANTARES: the first undersea neutrino telescope*, *Nucl. Instrum. Meth. A* **656** (2011) 11 [arXiv:1104.1607] [INSPIRE].

[78] KM3NET collaboration, *Letter of intent for KM3NeT 2.0*, *J. Phys. G* **43** (2016) 084001 [arXiv:1601.07459] [INSPIRE].

[79] H.S. Zhao, *Analytical models for galactic nuclei*, *Mon. Not. Roy. Astron. Soc.* **278** (1996) 488 [astro-ph/9509122] [INSPIRE].

[80] H.C. Plummer, *On the problem of distribution in globular star clusters: (plate 8)*, *Mon. Not. Roy. Astron. Soc.* **71** (1911) 460 [INSPIRE].

[81] D.R. Hunter, *Derivation of the anisotropy profile, constraints on the local velocity dispersion, and implications for direct detection*, *JCAP* **02** (2014) 023 [arXiv:1311.0256] [INSPIRE].

[82] B.K. Dhar and L.L.R. Williams, *Surface mass density of the Einasto family of dark matter haloes: are they Sersic-like?*, *Mon. Not. Roy. Astron. Soc.* **405** (2010) 340 [arXiv:1112.3116] [INSPIRE].

[83] M. Baes and E. Van Hese, *Dynamical models with a general anisotropy profile*, *Astron. Astrophys.* **471** (2007) 419 [arXiv:0705.4109] [INSPIRE].

[84] M.G. Walker, E.W. Olszewski and M. Mateo, *Bayesian analysis of resolved stellar spectra: application to MMT/Hectochelle observations of the Draco dwarf spheroidal*, *Mon. Not. Roy. Astron. Soc.* **448** (2015) 2717 [arXiv:1503.02589].

[85] A.B. Pace and L.E. Strigari, *Scaling relations for dark matter annihilation and decay profiles in dwarf spheroidal galaxies*, *Mon. Not. Roy. Astron. Soc.* **482** (2019) 3480 [arXiv:1802.06811] [INSPIRE].

[86] M. Di Mauro, M. Stref and F. Calore, *Investigating the effect of Milky Way dwarf spheroidal galaxies extension on dark matter searches with Fermi-LAT data*, *Phys. Rev. D* **106** (2022) 123032 [arXiv:2212.06850] [INSPIRE].

JCAP03(2026)035

The Fermi-LAT collaboration, the HAWC collaboration, the H.E.S.S. collaboration, the MAGIC collaboration and the VERITAS collaboration

S. Abdollahi[a,1], L. Baldini[a,2], R. Bellazzini[a,3], B. Berenji[a,4], E. Bissaldi[a,5,6], R. Bonino[a,7,8], P. Bruel[a,9], S. Buson[a,10], E. Charles[a,11,*], A. W. Chen[a,12], S. Ciprini[a,13,14], M. Crnogorcevic[a,15,16], A. Cuoco[a,7,8], F. D'Ammando[a,17], A. de Angelis[a,18], M. Di Mauro[a,7,*], N. Di Lalla[a,11], L. Di Venere[a,6], A. Domínguez[a,19], S. J. Fegan[a,9], A. Fiori[a,2], P. Fusco[a,5,6], V. Gammaldi[a,20,21], F. Gargano[a,6], D. Gasparrini[a,13,14], F. Giacchino[a,14a,13], N. Giglietto[a,5,6], M. Giliberti[a,6,5], F. Giordano[a,5,6], M. Giroletti[a,17], I. A. Grenier[a,22], S. Guiriec[a,23,16], M. Gustafsson[a,24], E. Hays[a,16], J.W. Hewitt[a,25], D. Horan[a,9], H. Katagiri[a,26], M. Kuss[a,3], J. Li[a,27,28], F. Longo[a,29,30], F. Loparco[a,5,6], L. Lorusso[a,5,6], G. Martí-Devesa[a,31], M. N. Mazziotta[a,6], J. E. McEnery[a,16,15], I. Mereu[a,32,33], M. Meyer[a,34], P. F. Michelson[a,11], N. Mirabal[a,16,35], W. Mitthumsiri[a,36], T. Mizuno[a,37], A. Morselli[a,13], I. V. Moskalenko[a,11], M. Negro[a,35,16], N. Omodei[a,11], M. Orienti[a,17], E. Orlando[a,38,11], G. Panzarini[a,5,6], M. Persic[a,30,39], M. Pesce-Rollins[a,3], R. Pillera[a,5,6], T. A. Porter[a,11], G. Principe[a,29,30,17], S. Rainò[a,5,6], R. Rando[a,40,41,42], M. Razzano[a,2], O. Reimer[a,31], M. Sánchez-Conde[a,21,20], P. M. Saz Parkinson[a,43], D. Serini[a,6], D. J. Suson[a,44], D. F. Torres[a,45,46], G. Zaharijas[a,47], A. Albert[b,48], R. Alfaro[b,49], C. Alvarez[b,50], J.C. Arteaga-Velázquez[b,51], D. Avila Rojas[b,49], H.A. Ayala Solares[b,52], R. Babu[b,53], E. Belmont-Moreno[b,49], K.S. Caballero-Mora[b,50], T. Capistrán[b,54], A. Carramiñana[b,55], S. Casanova[b,56], O. Chaparro-Amaro[b,57], U. Cotti[b,51], J. Cotzomi[b,58], S. Coutiño de León[b,51,59], E. de la Fuente[b,60], R. Diaz Hernandez[b,55], B.L. Dingus[b,48], M.A. DuVernois[b,59], M. Durocher[b,48], J.C. Díaz-Vélez[b,60], K. Engel[b,61], C. Espinoza[b,49], K.L. Fan[b,61], N. Fraija[b,54], J.A. García-González[b,62], F. Garfias[b,54], M.M. González[b,54], J.A. Goodman[b,61], J.P. Harding[b,48,*], S. Hernandez[b,49], I. Herzog[b,53], J. Hinton[b,63], D. Huang[b,61], F. Hueyotl-Zahuantitla[b,50], P. Hüntemeyer[b,64], A. Iriarte[b,54], V. Joshi[b,65], S. Kaufmann[b,66], D. Kieda[b,67], G.J. Kunde[b,48], A. Lara[b,68], J. Lee[b,69], H. León Vargas[b,49], J.T. Linnemann[b,53], A.L. Longinotti[b,54], G. Luis-Raya[b,66], J. Lundeen[b,53], K. Malone[b,48], O. Martinez[b,58], J. Martínez-Castro[b,57], H. Martínez-Huerta[b,70], J.A. Matthews[b,71], P. Miranda-Romagnoli[b,72], J.A. Morales-Soto[b,51], E. Moreno[b,58], M. Mostafá[b,52], A. Nayerhoda[b,56], L. Nellen[b,73], M.U. Nisa[b,53], R. Noriega-Papaqui[b,72], L. Olivera-Nieto[b,63], N. Omodei[b,74], A. Peisker[b,53], Y. Pérez Araujo[b,54], E.G. Pérez-Pérez[b,66], C.D. Rho[b,69], D. Rosa-González[b,55], H. Salazar[b,58], D. Salazar-Gallegos[b,53,*], A. Sandoval[b,49], M. Schneider[b,61], J. Serna-Franco[b,49], A.J. Smith[b,61], Y. Son[b,69], R.W. Springer[b,67], O. Tibolla[b,66], K. Tollefson[b,53,*], I. Torres[b,55], R. Torres-Escobedo[b,75], R. Turner[b,64], F. Ureña-Mena[b,55], E. Varela[b,58], L. Villaseñor[b,58], X. Wang[b,64], I.J. Watson[b,69], K. Whitaker[b,52], E. Willox[b,61], S. Yu[b,52], S. Yun-Cárcamo[b,61], H. Zhou[b,75], F. Aharonian[c,76,77], F. Ait Benkhali[c,78], C. Armand[c,79,*], J. Aschersleben[c,80], M. Backes[c,81,82], V. Barbosa Martins[c,83], R. Batzofin[c,84], Y. Becherini[c,85,86], D. Berge[c,86,87], B. Bi[c,88], M. Böttcher[c,82], C. Boisson[c,89], J. Bolmont[c,90], M. de Bony de Lavergne[c,79], J. Borowska[c,87], M. Bouyahiaoui[c,77], F. Bradascio[c,91], M. Breuhaus[c,77], F. Brun[c,91], B. Bruno[c,92], T. Bulik[c,93], C. Burger-Scheidlin[c,76], S. Caroff[c,79], S. Casanova[c,94], R. Cecil[c,95], J. Celic[c,92], M. Cerruti[c,85], T. Chand[c,82], S. Chandra[c,82], A. Chen[c,96], J. Chibueze[c,82], O. Chibueze[c,82], G. Cotter[c,97], S. Dai[c,98], J. Damascene Mbarubucyeye[c,83], A. Dmytriiev[c,82], V. Doroshenko[c,88],

JCAP03(2026)035

J.-P. Ernenwein[c,99], G. Fichet de Clairfontaine[c,89], M. Filipovic[c,98], G. Fontaine[c,100], M. Füßling[c,83], S. Funk[c,92], S. Gabici[c,85], S. Ghafourizadeh[c,78], G. Giavitto[c,83], D. Glawion[c,92], J.F. Glicenstein[c,91], G. Grolleron[c,90], L. Haerer[c,77], J.A. Hinton[c,77], W. Hofmann[c,77], T. L. Holch[c,83], M. Holler[c,101], D. Horns[c,95], M. Jamrozy[c,102], F. Jankowsky[c,78], A. Jardin-Blicq[c,103], V. Joshi[c,92], I. Jung-Richardt[c,92], E. Kasai[c,81], K. Katarzyński[c,104], R. Khatoon[c,82], B. Khélifi[c,85], W. Kluźniak[c,105], Nu. Komin[c,96], D. Kostunin[c,83], R.G. Lang[c,92], S. Le Stum[c,99], F. Leitl[c,92], A. Lemière[c,85], M. Lemoine-Goumard[c,103], J.-P. Lenain[c,90], F. Leuschner[c,88], T. Lohse[c,87], A. Luashvili[c,89], I. Lypova[c,78], J. Mackey[c,76], D. Malyshev[c,88], D. Malyshev[c,92], V. Marandon[c,77], P. Marchegiani[c,96], R. Marx[c,78], M. Meyer[c,95], A. Mitchell[c,92], R. Moderski[c,105], A. Montanari[c,78], E. Moulin[c,91,*], K. Nakashima[c,92], M. de Naurois[c,100], J. Niemiec[c,94], A. Priyana Noel[c,102], L. Oakes[c,87,*], P. O'Brien[c,106], S. Ohm[c,83], L. Olivera-Nieto[c,77], E. de Ona Wilhelmi[c,83], M. Ostrowski[c,102], S. Panny[c,101], M. Panter[c,77], R.D. Parsons[c,87], V. Poireau[c,79,*], D.A. Prokhorov[c,107], G. Pühlhofer[c,88], A. Quirrenbach[c,78], P. Reichherzer[c,91], A. Reimer[c,101], O. Reimer[c,101], F. Rieger[c,77], L. Rinchiuso[c,91,*], G. Rowell[c,108], B. Rudak[c,105], V. Sahakian[c,109], S. Sailer[c,77], A. Santangelo[c,88], M. Sasaki[c,92], J. Schäfer[c,92], U. Schwanke[c,87], J.N.S. Shapopi[c,81], H. Sol[c,89], A. Specovius[c,92], S. Spencer[c,92], Ł. Stawarz[c,102], R. Steenkamp[c,81], S. Steinmassl[c,77], C. Steppa[c,84], I. Sushch[c,82], H. Suzuki[c,110], T. Takahashi[c,111], T. Tanaka[c,110], T. Tavernier[c,91], A.M. Taylor[c,83], R. Terrier[c,85], C. Thorpe-Morgan[c,88], C. van Eldik[c,92], M. Vecchi[c,80], J. Veh[c,92], C. Venter[c,82], J. Vink[c,107], T. Wach[c,92], S.J. Wagner[c,78], A. Wierzcholska[c,94], Yu Wun Wong[c,92], M. Zacharias[c,78,82], D. Zargaryan[c,76], A.A. Zdziarski[c,105], A. Zech[c,89], S. Zouari[c,85], N. Żywucka[c,82], H. Abe[d,112], S. Abe[d,112], V. A. Acciari[d,113], I. Agudo[d,114], T. Aniello[d,115], S. Ansoldi[d,116,154], L. A. Antonelli[d,115], A. Arbet Engels[d,117], C. Arcaro[d,118], M. Artero[d,119], K. Asano[d,112], D. Baack[d,120], A. Babić[d,121], A. Baquero[d,122], U. Barres de Almeida[d,123], J. A. Barrio[d,122], I. Batković[d,118], J. Baxter[d,112], J. Becerra González[d,113], W. Bednarek[d,124], E. Bernardini[d,118], M. Bernardos[d,114], J. Bernete[d,125], A. Berti[d,117], C. Bigongiari[d,115], A. Biland[d,126], O. Blanch[d,119], G. Bonnoli[d,115], Ž. Bošnjak[d,121], I. Burelli[d,116], G. Busetto[d,118], A. Campoy Ordaz[d,127], A. Carosi[d,115], R. Carosi[d,128], M. Carretero-Castrillo[d,129], A. J. Castro-Tirado[d,114], G. Ceribella[d,117], Y. Chai[d,117], A. Cifuentes[d,125], S. Cikota[d,121], E. Colombo[d,113], J. L. Contreras[d,122], J. Cortina[d,125], S. Covino[d,115], G. D'Amico[d,130], V. D'Elia[d,115], P. Da Vela[d,128,155], F. Dazzi[d,115], A. De Angelis[d,118], B. De Lotto[d,116], A. Del Popolo[d,131], M. Delfino[d,119,156], J. Delgado[d,119,156], C. Delgado Mendez[d,125], D. Depaoli[d,132], F. Di Pierro[d,132], L. Di Venere[d,133], D. Dominis Prester[d,134], A. Donini[d,115], D. Dorner[d,135], M. Doro[d,118], D. Elsaesser[d,120], G. Emery[d,136], J. Escudero[d,114], L. Fariña[d,119], A. Fattorini[d,120], L. Foffano[d,115], L. Font[d,127], S. Fröse[d,120], S. Fukami[d,126], Y. Fukazawa[d,137], R. J. García López[d,113], M. Garczarczyk[d,138], S. Gasparyan[d,139], M. Gaug[d,127], J. G. Giesbrecht Paiva[d,123], N. Giglietto[d,133], F. Giordano[d,133], P. Gliwny[d,124], N. Godinović[d,140], R. Grau[d,119], D. Green[d,117], J. G. Green[d,117], D. Hadasch[d,112], A. Hahn[d,117], T. Hassan[d,125], L. Heckmann[d,117,157], J. Herrera[d,113], D. Hrupec[d,141], M. Hütten[d,112], R. Imazawa[d,137], T. Inada[d,112], R. Iotov[d,135], K. Ishio[d,124], I. Jiménez Martínez[d,125], J. Jormanainen[d,142], D. Kerszberg[d,119,158,*], G. W. Kluge[d,130,159],

JCAP03(2026)035

Y. Kobayashi[d,112], P. M. Kouch[d,142], H. Kubo[d,112], J. Kushida[d,143], M. Láinez Lezáun[d,122], A. Lamastra[d,115], F. Leone[d,115], E. Lindfors[d,142], S. Lombardi[d,115], F. Longo[d,116,160], R. López-Coto[d,114], M. López-Moya[d,122], A. López-Oramas[d,113], S. Loporchio[d,133], A. Lorini[d,144], B. Machado de Oliveira Fraga[d,123], P. Majumdar[d,145], M. Makariev[d,146], G. Maneva[d,146], N. Mang[d,120], M. Manganaro[d,134], S. Mangano[d,125], K. Mannheim[d,135], M. Mariotti[d,118], M. Martínez[d,119], A. Mas-Aguilar[d,122], D. Mazin[d,112,117], S. Menchiari[d,144], S. Mender[d,120], D. Miceli[d,118], T. Miener[d,122,161,*], J. M. Miranda[d,144], R. Mirzoyan[d,117], M. Molero González[d,113], E. Molina[d,113], H. A. Mondal[d,145], A. Moralejo[d,119], D. Morcuende[d,122], C. Nanci[d,115], V. Neustroev[d,147], M. Nievas Rosillo[d,113], C. Nigro[d,119], K. Nilsson[d,142], K. Nishijima[d,143], T. Njoh Ekoume[d,113], K. Noda[d,148], S. Nozaki[d,117], Y. Ohtani[d,112], A. Okumura[d,149], J. Otero-Santos[d,113], S. Paiano[d,115], M. Palatiello[d,116], D. Paneque[d,117], R. Paoletti[d,144], J. M. Paredes[d,129], L. Pavletić[d,134], M. Persic[d,116,162], M. Pihet[d,118], G. Pirola[d,117], F. Podobnik[d,144], P. G. Prada Moroni[d,128], E. Prandini[d,118], G. Principe[d,116], C. Priyadarshi[d,119], W. Rhode[d,120], M. Ribó[d,129], J. Rico[d,119,*], C. Righi[d,125], N. Sahakyan[d,139], T. Saito[d,112], K. Satalecka[d,142], F. G. Saturni[d,115], B. Schleicher[d,135], K. Schmidt[d,120], F. Schmuckermaier[d,117], J. L. Schubert[d,120], T. Schweizer[d,117], A. Sciaccaluga[d,115], J. Sitarek[d,124], V. Sliusar[d,136], D. Sobczynska[d,124], A. Spolon[d,118], A. Stamerra[d,125], J. Strišković[d,141], D. Strom[d,117], M. Strzys[d,112], Y. Suda[d,137], S. Suutarinen[d,142], H. Tajima[d,149], M. Takahashi[d,149], R. Takeishi[d,112], F. Tavecchio[d,115], P. Temnikov[d,146], K. Terauchi[d,150], T. Terzić[d,134], M. Teshima[d,117,112], L. Tosti[d,151], S. Truzzi[d,144], A. Tutone[d,115], S. Ubach[d,127], J. van Scherpenberg[d,117], M. Vazquez Acosta[d,113], S. Ventura[d,144], V. Verguilov[d,146], I. Viale[d,118], C. F. Vigorito[d,132], V. Vitale[d,152], I. Vovk[d,112], R. Walter[d,136], M. Will[d,117], C. Wunderlich[d,144], T. Yamamoto[d,153], A. Acharyya[e,163], C. B. Adams[e,164], A. Archer[e,165], P. Bangale[e,166], J. T. Bartkoske[e,167], P. Batista[e,168], W. Benbow[e,169], J. H. Buckley[e,170], Y. Chen[e,171], J. L. Christiansen[e,172], A. J. Chromey[e,169], M. Errando[e,170], M. Escobar Godoy[e,173], A. Falcone[e,174], S. Feldman[e,171], Q. Feng[e,167], J. P. Finley[e,175], G. M. Foote[e,166], L. Fortson[e,176], A. Furniss[e,173], G. Gallagher[e,177], C. Giuri[e,168,*], W. Hanlon[e,169], O. Hervet[e,173], C. E. Hinrichs[e,169,178], J. Hoang[e,173], J. Holder[e,166], Z. Hughes[e,170], T. B. Humensky[e,179,180], W. Jin[e,171], M. N. Johnson[e,173], P. Kaaret[e,181], M. Kertzman[e,165], M. Kherlakian[e,182], D. Kieda[e,167], T. K. Kleiner[e,168], N. Korzoun[e,166], F. Krennrich[e,183], S. Kumar[e,179], M. Lundy[e,184], G. Maier[e,168], C. E McGrath[e,185], M. J. Millard[e,181], J. Millis[e,177], C. L. Mooney[e,166], P. Moriarty[e,186], R. Mukherjee[e,187], D. Nieto[e,188], S. O'Brien[e,184,189], R. A. Ong[e,171], M. Pohl[e,190,168], E. Pueschel[e,182,*], J. Quinn[e,185], P. L. Rabinowitz[e,170], K. Ragan[e,184], P. T. Reynolds[e,191], D. Ribeiro[e,176], E. Roache[e,169], J. L. Ryan[e,171], I. Sadeh[e,168], L. Saha[e,169], M. Santander[e,192], G. H. Sembroski[e,175], R. Shang[e,187], M. Splettstoesser[e,173], D. Tak[e,193], A. K. Talluri[e,176], J. V. Tucci[e,194], V. V. Vassiliev[e,171], A. Weinstein[e,183], D. A. Williams[e,173], S. L. Wong[e,184]

[1] *IRAP, Université de Toulouse, CNRS, UPS, CNES, F-31028 Toulouse, France*

[2] *Università di Pisa and Istituto Nazionale di Fisica Nucleare, Sezione di Pisa I-56127 Pisa, Italy*

[3] *Istituto Nazionale di Fisica Nucleare, Sezione di Pisa, I-56127 Pisa, Italy*

[4] *California State University, Los Angeles, Department of Physics and Astronomy, Los Angeles, CA 90032, U.S.A.*

[5] *Dipartimento di Fisica "M. Merlin" dell'Università e del Politecnico di Bari, via Amendola 173, I-70126 Bari, Italy*

JCAP03(2026)035

[6] *Istituto Nazionale di Fisica Nucleare, Sezione di Bari, I-70126 Bari, Italy*
[7] *Istituto Nazionale di Fisica Nucleare, Sezione di Torino, I-10125 Torino, Italy*
[8] *Dipartimento di Fisica, Università degli Studi di Torino, I-10125 Torino, Italy*
[9] *Laboratoire Leprince-Ringuet, CNRS/IN2P3, École polytechnique, Institut Polytechnique de Paris, 91120 Palaiseau, France*
[10] *Institut für Theoretische Physik and Astrophysik, Universität Würzburg, D-97074 Würzburg, Germany*
[11] *W. W. Hansen Experimental Physics Laboratory, Kavli Institute for Particle Astrophysics and Cosmology, Department of Physics and SLAC National Accelerator Laboratory, Stanford University, Stanford, CA 94305, U.S.A.*
[12] *School of Physics, University of the Witwatersrand, Private Bag 3, WITS-2050, Johannesburg, South Africa*
[13] *Istituto Nazionale di Fisica Nucleare, Sezione di Roma "Tor Vergata", I-00133 Roma, Italy*
[14] *Space Science Data Center — Agenzia Spaziale Italiana, Via del Politecnico, snc, I-00133, Roma, Italy*
[14a] *Department of Fundamental Physics, University of Salamanca, Plaza de la Merced s/n, E-37008 Salamanca, Spain*
[15] *Department of Astronomy, University of Maryland, College Park, MD 20742, U.S.A.*
[16] *NASA Goddard Space Flight Center, Greenbelt, MD 20771, U.S.A.*
[17] *INAF Istituto di Radioastronomia, I-40129 Bologna, Italy*
[18] *Dipartimento di Fisica, Università di Udine and Istituto Nazionale di Fisica Nucleare, Sezione di Trieste, Gruppo Collegato di Udine, I-33100 Udine, Italy*
[19] *Grupo de Altas Energías, Universidad Complutense de Madrid, E-28040 Madrid, Spain*
[20] *Departamento de Física Teórica, Universidad Autónoma de Madrid, 28049 Madrid, Spain*
[21] *Instituto de Física Teórica UAM/CSIC, Universidad Autónoma de Madrid, E-28049 Madrid, Spain*
[22] *Université Paris Cité, Université Paris-Saclay, CEA, CNRS, AIM, F-91191 Gif-sur-Yvette, France*
[23] *The George Washington University, Department of Physics, 725 21st St, NW, Washington, DC 20052, U.S.A.*
[24] *Georg-August University Göttingen, Institute for theoretical Physics — Faculty of Physics, Friedrich-Hund-Platz 1, D-37077 Göttingen, Germany*
[25] *University of North Florida, Department of Physics, 1 UNF Drive, Jacksonville, FL 32224, U.S.A.*
[26] *College of Science, Ibaraki University, 2-1-1, Bunkyo, Mito 310-8512, Japan*
[27] *CAS Key Laboratory for Research in Galaxies and Cosmology, Department of Astronomy, University of Science and Technology of China, Hefei 230026, People's Republic of China*
[28] *School of Astronomy and Space Science, University of Science and Technology of China, Hefei 230026, People's Republic of China*
[29] *Dipartimento di Fisica, Università di Trieste, I-34127 Trieste, Italy*
[30] *Istituto Nazionale di Fisica Nucleare, Sezione di Trieste, I-34127 Trieste, Italy*
[31] *Institut für Astro- und Teilchenphysik, Leopold-Franzens-Universität Innsbruck, A-6020 Innsbruck, Austria*
[32] *Istituto Nazionale di Fisica Nucleare, Sezione di Perugia, I-06123 Perugia, Italy*
[33] *Dipartimento di Fisica, Università degli Studi di Perugia, I-06123 Perugia, Italy*
[34] *Center for Cosmology and Particle Physics Phenomenology, University of Southern Denmark, Campusvej 55, DK-5230 Odense M, Denmark*
[35] *Department of Physics and Center for Space Sciences and Technology, University of Maryland Baltimore County, Baltimore, MD 21250, U.S.A.*
[36] *Department of Physics, Faculty of Science, Mahidol University, Bangkok 10400, Thailand*
[37] *Hiroshima Astrophysical Science Center, Hiroshima University, Higashi-Hiroshima, Hiroshima 739-8526, Japan*
[38] *Istituto Nazionale di Fisica Nucleare, Sezione di Trieste, and Università di Trieste, I-34127 Trieste, Italy*
[39] *INAF-Astronomical Observatory of Padova, Vicolo dell'Osservatorio 5, I-35122 Padova, Italy*
[40] *Dipartimento di Fisica e Astronomia "G. Galilei", Università di Padova, Via F. Marzolo, 8, I-35131 Padova, Italy*
[41] *Istituto Nazionale di Fisica Nucleare, Sezione di Padova, I-35131 Padova, Italy*
[42] *Center for Space Studies and Activities "G. Colombo", University of Padova, Via Venezia 15, I-35131 Padova, Italy*

JCAP03(2026)035

[43] Santa Cruz Institute for Particle Physics, Department of Physics and Department of Astronomy and Astrophysics, University of California at Santa Cruz, Santa Cruz, CA 95064, U.S.A.
[44] Purdue University Northwest, Hammond, IN 46323, U.S.A.
[45] Institute of Space Sciences (ICE, CSIC), Campus UAB, Carrer de Magrans s/n, E-08193 Barcelona, Spain; and Institut d'Estudis Espacials de Catalunya (IEEC), E-08034 Barcelona, Spain
[46] Institució Catalana de Recerca i Estudis Avançats (ICREA), E-08010 Barcelona, Spain
[47] Center for Astrophysics and Cosmology, University of Nova Gorica, Nova Gorica, Slovenia
[48] Los Alamos National Laboratory, Los Alamos, NM, U.S.A.
[49] Instituto de Física, Universidad Nacional Autónoma de México, Ciudad de Mexico, Mexico
[50] Universidad Autónoma de Chiapas, Tuxtla Gutiérrez, Chiapas, México
[51] Universidad Michoacana de San Nicolás de Hidalgo, Morelia, Mexico
[52] Department of Physics, Pennsylvania State University, University Park, PA, U.S.A.
[53] Department of Physics and Astronomy, Michigan State University, East Lansing, MI, U.S.A.
[54] Instituto de Astronomía, Universidad Nacional Autónoma de México, Ciudad de Mexico, Mexico
[55] Instituto Nacional de Astrofísica, Óptica y Electrónica, Puebla, Mexico
[56] Institute of Nuclear Physics Polish Academy of Sciences, PL-31342 IFJ-PAN, Krakow, Poland
[57] Centro de Investigación en Computación, Instituto Politécnico Nacional, México City, México
[58] Facultad de Ciencias Físico Matemáticas, Benemérita Universidad Autónoma de Puebla, Puebla, Mexico
[59] Department of Physics, University of Wisconsin-Madison, Madison, WI, U.S.A.
[60] Departamento de Física, Centro Universitario de Ciencias Exactase Ingenierias, Universidad de Guadalajara, Guadalajara, Mexico
[61] Department of Physics, University of Maryland, College Park, MD, U.S.A.
[62] Tecnologico de Monterrey, Escuela de Ingeniería y Ciencias, Ave. Eugenio Garza Sada 2501, Monterrey, N.L., Mexico, 64849
[63] Max-Planck Institute for Nuclear Physics, 69117 Heidelberg, Germany
[64] Department of Physics, Michigan Technological University, Houghton, MI, U.S.A.
[65] Erlangen Centre for Astroparticle Physics, Friedrich-Alexander-Universität Erlangen-Nürnberg, Erlangen, Germany
[66] Universidad Politecnica de Pachuca, Pachuca, Hgo, Mexico
[67] Department of Physics and Astronomy, University of Utah, Salt Lake City, UT, U.S.A.
[68] Instituto de Geofísica, Universidad Nacional Autónoma de México, Ciudad de Mexico, Mexico
[69] University of Seoul, Seoul, Rep. of Korea
[70] Departamento de Física y Matemáticas, Universidad de Monterrey, Av. Morones Prieto 4500, San Pedro Garza García 66238, Nuevo León, Mexico
[71] Dept of Physics and Astronomy, University of New Mexico, Albuquerque, NM, U.S.A.
[72] Universidad Autónoma del Estado de Hidalgo, Pachuca, Mexico
[73] Instituto de Ciencias Nucleares, Universidad Nacional Autónoma de Mexico, Ciudad de Mexico, Mexico
[74] Department of Physics, Stanford University: Stanford, CA 94305–4060, U.S.A.
[75] Tsung-Dao Lee Institute and School of Physics and Astronomy, Shanghai Jiao Tong University, Shanghai, China
[76] Dublin Institute for Advanced Studies, 31 Fitzwilliam Place, Dublin 2, Ireland
[77] Max-Planck-Institut für Kernphysik, P.O. Box 103980, D 69029 Heidelberg, Germany
[78] Landessternwarte, Universität Heidelberg, Königstuhl, D 69117 Heidelberg, Germany
[79] Université Savoie Mont Blanc, CNRS, Laboratoire d'Annecy de Physique des Particules — IN2P3, 74000 Annecy, France
[80] Kapteyn Astronomical Institute, University of Groningen, Landleven 12, 9747 AD Groningen, The Netherlands
[81] University of Namibia, Department of Physics, Private Bag 13301, Windhoek 10005, Namibia
[82] Centre for Space Research, North-West University, Potchefstroom 2520, South Africa
[83] DESY, D-15738 Zeuthen, Germany
[84] Institut für Physik und Astronomie, Universität Potsdam, Karl-Liebknecht-Strasse 24/25, D 14476 Potsdam, Germany
[85] Université de Paris, CNRS, Astroparticule et Cosmologie, F-75013 Paris, France

JCAP03(2026)035

[86] Department of Physics and Electrical Engineering, Linnaeus University, 351 95 Växjö, Sweden
[87] Institut für Physik, Humboldt-Universität zu Berlin, Newtonstr. 15, D 12489 Berlin, Germany
[88] Institut für Astronomie und Astrophysik, Universität Tübingen, Sand 1, D 72076 Tübingen, Germany
[89] Laboratoire Univers et Théories, Observatoire de Paris, Université PSL, CNRS, Université de Paris, 92190 Meudon, France
[90] Sorbonne Université, CNRS/IN2P3, Laboratoire de Physique Nucléaire et de Hautes Energies, LPNHE, 4 place Jussieu, 75005 Paris, France
[91] IRFU, CEA, Université Paris-Saclay, F-91191 Gif-sur-Yvette, France
[92] Friedrich-Alexander-Universität Erlangen-Nürnberg, Erlangen Centre for Astroparticle Physics, Erwin-Rommel-Str. 1, D 91058 Erlangen, Germany
[93] Astronomical Observatory, The University of Warsaw, Al. Ujazdowskie 4, 00-478 Warsaw, Poland
[94] Instytut Fizyki Jądrowej PAN, ul. Radzikowskiego 152, 31-342 Kraków, Poland
[95] Universität Hamburg, Institut für Experimentalphysik, Luruper Chaussee 149, D 22761 Hamburg, Germany
[96] School of Physics, University of the Witwatersrand, 1 Jan Smuts Avenue, Braamfontein, Johannesburg, 2050 South Africa
[97] University of Oxford, Department of Physics, Denys Wilkinson Building, Keble Road, Oxford OX1 3RH, U.K.
[98] School of Science, Western Sydney University, Locked Bag 1797, Penrith South DC, NSW 2751, Australia
[99] Aix Marseille Université, CNRS/IN2P3, CPPM, Marseille, France
[100] Laboratoire Leprince-Ringuet, École Polytechnique, CNRS, Institut Polytechnique de Paris, F-91128 Palaiseau, France
[101] Leopold-Franzens-Universität Innsbruck, Institut für Astro- und Teilchenphysik, A-6020 Innsbruck, Austria
[102] Obserwatorium Astronomiczne, Uniwersytet Jagielloński, ul. Orla 171, 30-244 Kraków, Poland
[103] Université Bordeaux, CNRS, LP2I Bordeaux, UMR 5797, F-33170 Gradignan, France
[104] Institute of Astronomy, Faculty of Physics, Astronomy and Informatics, Nicolaus Copernicus University, Grudziadzka 5, 87-100 Torun, Poland
[105] Nicolaus Copernicus Astronomical Center, Polish Academy of Sciences, ul. Bartycka 18, 00-716 Warsaw, Poland
[106] Department of Physics and Astronomy, The University of Leicester, University Road, Leicester, LE1 7RH, United Kingdom
[107] GRAPPA, Anton Pannekoek Institute for Astronomy, University of Amsterdam, Science Park 904, 1098 XH Amsterdam, The Netherlands
[108] School of Physical Sciences, University of Adelaide, Adelaide 5005, Australia
[109] Yerevan Physics Institute, 2 Alikhanian Brothers St., 375036 Yerevan, Armenia
[110] Department of Physics, Konan University, 8-9-1 Okamoto, Higashinada, Kobe, Hyogo 658-8501, Japan
[111] Kavli Institute for the Physics and Mathematics of the Universe (WPI), The University of Tokyo Institutes for Advanced Study (UTIAS), The University of Tokyo, 5-1-5 Kashiwa-no-Ha, Kashiwa, Chiba, 277-8583, Japan
[112] Japanese MAGIC Group: Institute for Cosmic Ray Research (ICRR), The University of Tokyo, Kashiwa, 277-8582 Chiba, Japan
[113] Instituto de Astrofísica de Canarias and Dpto. de Astrofísica, Universidad de La Laguna, E-38200, La Laguna, Tenerife, Spain
[114] Instituto de Astrofísica de Andalucía-CSIC, Glorieta de la Astronomía s/n, 18008, Granada, Spain
[115] National Institute for Astrophysics (INAF), I-00136 Rome, Italy
[116] Università di Udine and INFN Trieste, I-33100 Udine, Italy
[117] Max-Planck-Institut für Physik, D-80805 München, Germany
[118] Università di Padova and INFN, I-35131 Padova, Italy
[119] Institut de Física d'Altes Energies (IFAE), The Barcelona Institute of Science and Technology (BIST), E-08193 Bellaterra (Barcelona), Spain
[120] Technische Universität Dortmund, D-44221 Dortmund, Germany
[121] Croatian MAGIC Group: University of Zagreb, Faculty of Electrical Engineering and Computing (FER), 10000 Zagreb, Croatia

JCAP03(2026)035

[122] *IPARCOS Institute and EMFTEL Department, Universidad Complutense de Madrid, E-28040 Madrid, Spain*
[123] *Centro Brasileiro de Pesquisas Físicas (CBPF), 22290-180 URCA, Rio de Janeiro (RJ), Brazil*
[124] *University of Lodz, Faculty of Physics and Applied Informatics, Department of Astrophysics, 90-236 Lodz, Poland*
[125] *Centro de Investigaciones Energéticas, Medioambientales y Tecnológicas, E-28040 Madrid, Spain*
[126] *ETH Zürich, CH-8093 Zürich, Switzerland*
[127] *Departament de Física, and CERES-IEEC, Universitat Autònoma de Barcelona, E-08193 Bellaterra, Spain*
[128] *Università di Pisa and INFN Pisa, I-56126 Pisa, Italy*
[129] *Universitat de Barcelona, ICCUB, IEEC-UB, E-08028 Barcelona, Spain*
[130] *Department for Physics and Technology, University of Bergen, Norway*
[131] *INFN MAGIC Group: INFN Sezione di Catania and Dipartimento di Fisica e Astronomia, University of Catania, I-95123 Catania, Italy*
[132] *INFN MAGIC Group: INFN Sezione di Torino and Università degli Studi di Torino, I-10125 Torino, Italy*
[133] *INFN MAGIC Group: INFN Sezione di Bari and Dipartimento Interateneo di Fisica dell'Università e del Politecnico di Bari, I-70125 Bari, Italy*
[134] *Croatian MAGIC Group: University of Rijeka, Faculty of Physics, 51000 Rijeka, Croatia*
[135] *Universität Würzburg, D-97074 Würzburg, Germany*
[136] *University of Geneva, Chemin d'Ecogia 16, CH-1290 Versoix, Switzerland*
[137] *Japanese MAGIC Group: Physics Program, Graduate School of Advanced Science and Engineering, Hiroshima University, 739-8526 Hiroshima, Japan*
[138] *Deutsches Elektronen-Synchrotron (DESY), D-15738 Zeuthen, Germany*
[139] *Armenian MAGIC Group: ICRANet-Armenia, 0019 Yerevan, Armenia*
[140] *Croatian MAGIC Group: University of Split, Faculty of Electrical Engineering, Mechanical Engineering and Naval Architecture (FESB), 21000 Split, Croatia*
[141] *Croatian MAGIC Group: Josip Juraj Strossmayer University of Osijek, Department of Physics, 31000 Osijek, Croatia*
[142] *Finnish MAGIC Group: Finnish Centre for Astronomy with ESO, University of Turku, FI-20014 Turku, Finland*
[143] *Japanese MAGIC Group: Department of Physics, Tokai University, Hiratsuka, 259-1292 Kanagawa, Japan*
[144] *Università di Siena and INFN Pisa, I-53100 Siena, Italy*
[145] *Saha Institute of Nuclear Physics, A CI of Homi Bhabha National Institute, Kolkata 700064, West Bengal, India*
[146] *Inst. for Nucl. Research and Nucl. Energy, Bulgarian Academy of Sciences, BG-1784 Sofia, Bulgaria*
[147] *Finnish MAGIC Group: Space Physics and Astronomy Research Unit, University of Oulu, FI-90014 Oulu, Finland*
[148] *Japanese MAGIC Group: Chiba University, ICEHAP, 263-8522 Chiba, Japan*
[149] *Japanese MAGIC Group: Institute for Space-Earth Environmental Research and Kobayashi-Maskawa Institute for the Origin of Particles and the Universe, Nagoya University, 464-6801 Nagoya, Japan*
[150] *Japanese MAGIC Group: Department of Physics, Kyoto University, 606-8502 Kyoto, Japan*
[151] *INFN MAGIC Group: INFN Sezione di Perugia, I-06123 Perugia, Italy*
[152] *INFN MAGIC Group: INFN Roma Tor Vergata, I-00133 Roma, Italy*
[153] *Japanese MAGIC Group: Department of Physics, Konan University, Kobe, Hyogo 658-8501, Japan*
[154] *Also at International Center for Relativistic Astrophysics (ICRA), Rome, Italy*
[155] *Now at Institute for Astro- and Particle Physics, University of Innsbruck, A-6020 Innsbruck, Austria*
[156] *Also at Port d'Informació Científica (PIC), E-08193 Bellaterra (Barcelona), Spain*
[157] *Also at Institute for Astro- and Particle Physics, University of Innsbruck, A-6020 Innsbruck, Austria*
[158] *Now at Sorbonne Université, CNRS/IN2P3, Laboratoire de Physique Nucléaire et de Hautes Energies, LPNHE, 4 place Jussieu, 75005 Paris, France*
[159] *Also at Department of Physics, University of Oslo, Norway*
[160] *Also at Dipartimento di Fisica, Università di Trieste, I-34127 Trieste, Italy*

JCAP03(2026)035

[161] *Now at Département de physique nucléaire et corpusculaire, University de Genève, Faculté de Sciences, 1205 Genève, Switzerland*
[162] *Also at INAF Padova*
[163] *CP3-Origins, University of Southern Denmark, Campusvej 55, 5230 Odense M, Denmark*
[164] *Physics Department, Columbia University, New York, NY 10027, U.S.A.*
[165] *Department of Physics and Astronomy, DePauw University, Greencastle, IN 46135-0037, U.S.A.*
[166] *Department of Physics and Astronomy and the Bartol Research Institute, University of Delaware, Newark, DE 19716, U.S.A.*
[167] *Department of Physics and Astronomy, University of Utah, Salt Lake City, UT 84112, U.S.A.*
[168] *DESY, Platanenallee 6, 15738 Zeuthen, Germany*
[169] *Center for Astrophysics | Harvard & Smithsonian, Cambridge, MA 02138, U.S.A.*
[170] *Department of Physics, Washington University, St. Louis, MO 63130, U.S.A.*
[171] *Department of Physics and Astronomy, University of California, Los Angeles, CA 90095, U.S.A.*
[172] *Physics Department, California Polytechnic State University, San Luis Obispo, CA 94307, U.S.A.*
[173] *Santa Cruz Institute for Particle Physics and Department of Physics, University of California, Santa Cruz, CA 95064, U.S.A.*
[174] *Department of Astronomy and Astrophysics, 525 Davey Lab, Pennsylvania State University, University Park, PA 16802, U.S.A.*
[175] *Department of Physics and Astronomy, Purdue University, West Lafayette, IN 47907, U.S.A.*
[176] *School of Physics and Astronomy, University of Minnesota, Minneapolis, MN 55455, U.S.A.*
[177] *Department of Physics and Astronomy, Ball State University, Muncie, IN 47306, U.S.A.*
[178] *Department of Physics and Astronomy, Dartmouth College, 6127 Wilder Laboratory, Hanover, NH 03755 U.S.A.*
[179] *Department of Physics, University of Maryland, College Park, MD, U.S.A.*
[180] *NASA GSFC, Greenbelt, MD 20771, U.S.A.*
[181] *Department of Physics and Astronomy, University of Iowa, Van Allen Hall, Iowa City, IA 52242, U.S.A.*
[182] *Fakultät für Physik & Astronomie, Ruhr-Universität Bochum, D-44780 Bochum, Germany*
[183] *Department of Physics and Astronomy, Iowa State University, Ames, IA 50011, U.S.A.*
[184] *Physics Department, McGill University, Montreal, QC H3A 2T8, Canada*
[185] *School of Physics, University College Dublin, Belfield, Dublin 4, Ireland*
[186] *School of Natural Sciences, University of Galway, University Road, Galway, H91 TK33, Ireland*
[187] *Department of Physics and Astronomy, Barnard College, Columbia University, NY 10027, U.S.A.*
[188] *Institute of Particle and Cosmos Physics, Universidad Complutense de Madrid, 28040 Madrid, Spain*
[189] *Arthur B. McDonald Canadian Astroparticle Physics Research Institute, 64 Bader Lane, Queen's University, Kingston, ON Canada, K7L 3N6*
[190] *Institute of Physics and Astronomy, University of Potsdam, 14476 Potsdam-Golm, Germany*
[191] *Department of Physical Sciences, Munster Technological University, Bishopstown, Cork, T12 P928, Ireland*
[192] *Department of Physics and Astronomy, University of Alabama, Tuscaloosa, AL 35487, U.S.A.*
[193] *SNU Astronomy Research Center, Seoul National University, Seoul 08826, Republic of Korea*
[194] *Department of Physics, Indiana University-Purdue University Indianapolis, Indianapolis, IN 46202, U.S.A.*

[*] *Corresponding author*
[a] *Member of the* Fermi-*LAT collaboration.*
[b] *Member of the HAWC collaboration.*
[c] *Member of the H.E.S.S. collaboration.*
[d] *Member of the MAGIC collaboration.*
[e] *Member of the VERITAS collaboration.*

JCAP03(2026)035